Calculations of electron inelastic mean free paths. XIII. Data for 14 organic compounds and water over the 50 eV to 200 keV range with the relativistic full Penn algorithm.

Hiroshi Shinotsuka,[1] Shigeo Tanuma,[1*] and Cedric J. Powell[2]

[1]Materials Data Platform Center, National Institute for Materials Science, 1-1 Namiki, Tsukuba, Ibaraki 305-0044, Japan

[2] Associate, Materials Measurement Science Division, National Institute of Standards and Technology, Gaithersburg, MD 20899-8370, USA

ABSTRACT

We have calculated inelastic mean free paths (IMFPs) for 14 organic compounds (26-n-paraffin, adenine, β-carotene, diphenyl-hexatriene, guanine, Kapton, polyacetylene, poly(butene-1-sulfone), polyethylene, polymethylmethacrylate, polystyrene, poly(2-vinylpridine), thymine, and uracil) and liquid water for electron energies from 50 eV to 200 keV with the relativistic full Pen algorithm including the correction of the bandgap effect in insulators. These calculations were made with energy-loss functions (ELFs) obtained from measured optical constants and from calculated atomic scattering factors for X-ray energies. Our calculated IMFPs could be fitted to a modified form of the relativistic Bethe equation for inelastic scattering of electrons in matter from 50 eV to

[*] *Correspondence to*: Shigeo Tanuma, Materials Data Platform Center ,National Institute for Materials Science, 1-1 Namiki, Tsukuba, Ibaraki 305-0044, Japan.
E-mail: tanuma.shigeo@nims.go.jp

200 keV. The average root-mean-square (RMS) deviation in these fits was 0.17 %. The IMFPs were also compared with a relativistic version of our predictive Tanuma-Powell-Penn (TPP-2M) equation. The average RMS deviation in these comparisons was 7.2 % for energies between 50 eV and 200 keV. This average RMS deviation is lower than that found in a similar comparison for our group of 41 elemental solids (11.9 %) and for our group of 42 inorganic compounds (10.7%) for the same energy range. We found generally satisfactory agreement between our calculated IMFPs and values from other calculations for energies between 200 eV and 10 keV. We also found reasonable agreement between our IMFPs for organic compounds and measured IMFPs for energies between 50 eV and 200 keV. Substantial progress for IMFP measurements for liquid water has been made in recent years through the invention of liquid-water microjet photoelectron spectroscopy and droplet photoelectron imaging. We found that the IMFPs from these experiments and the associated analyses were larger than our IMFPs by factors between two and four for energies between about 30 eV and 1000 eV. The energy dependences of the measured IMFPs are, however, similar to that of our IMFPs in the same energy range. Since IMFPs calculated from the same algorithm for a number of inorganic compounds agree reasonably well with measured IMFPs for energies between 100 eV and 200 keV, the large differences between IMFPs for water from recent experiments and our results are surprising and need to be resolved with additional experiments.

1. Introduction

Information on the inelastic scattering of electrons in solids is important in various applications ranging from radiation physics and radiation transport to thin-film analysis in the transmission electron microscope (TEM) and surface analysis by Auger-electron spectroscopy (AES) and X-ray photoelectron spectroscopy (XPS). A key parameter in these applications is the electron inelastic mean free path (IMFP), λ, which is simply related to the total cross section for inelastic scattering, σ, and the number density of atoms per unit volume in the solid, N: $\lambda = (\sigma N)^{-1}$.

We have calculated IMFPs for many solid materials over a wide range of electron energies.[1,2,3,4,5,6,7,8] Initially, we reported IMFPs for 50 eV to 2,000 eV electrons for 27 elemental solids,[1,2] 15 inorganic compounds,[3] and 14 organic compounds.[4] We later calculated IMFPs for 41 elemental solids[5] for energies up to 30 keV due to the growing interest in XPS and related experiments performed with X-rays of much higher energies for both scientific and industrial purposes. These IMFPs were calculated from experimental optical data with the non-relativistic full Penn algorithm (FPA)[9] for electron energies under 200 eV and the single-pole approximation or simple Penn algorithm (SPA)[9] for higher energies. We analyzed these calculated IMFPs with the modified Bethe equation for inelastic scattering of electrons in matter[10] to develop an IMFP predictive formula (designated TPP-2M).[4] The TPP-2M equation could be used to estimate IMFPs in other materials for energies between 50 eV and 2,000 eV, the energy range of interest for many AES and XPS experiments.

We extended our IMFP calculations for electron energies up to 200 keV with a relativistic version of the FPA for applications of thin-film analysis by TEM.[6] We first calculated IMFPs in 41 elemental solids[6] for energies from 50 eV to 200 keV and then

calculated IMFPs in 42 inorganic compounds.[8] In the latter work, we utilized the approach of Boutboul *et al.*[11] to include the effect of the bandgap energy for nonconductors in the IMFP calculation. In addition, we developed a relativistic version of the TPP-2M equation that provides reasonable IMFP estimates for energies between 50 eV and 200 keV.[6] The root-mean-square (RMS) deviation between the estimated IMFPs from the TPP-2M equation and the directly calculated values was 11.9 % for the group of 41 elemental solids.[8] This RMS deviation was similar to that found (10.2 %) in a similar comparison with the original non-relativistic TPP-2M equation for our original group of 27 elemental solids for the 50 eV to 2 keV energy range.[6] In another comparison, we found a 10.7 % RMS deviation between our calculated IMFPs for 42 inorganic compounds and the corresponding values from the relativistic TPP-2M equation for energies between 50 eV and 200 keV.[8]

In this paper, we extend our previous calculations[4] of IMFPs for 14 organic compounds and electron energies between 50 eV and 2,000 eV. We report here new calculations of IMFPs with the relativistic FPA[8] using the Boutboul *et al.* approach, which we designate as FPA-BABC, for 14 organic compounds (26-n-paraffin, adenine, β-carotene, diphenyl-hexatriene (DPHT), guanine, Kapton, polyacetylene (PA), poly(butene-1-sulfone) (PBS), polyethylene (PE), polymethylmethacrylate (PMMA), polystyrene (PS), poly(2-vinylpridine) (P2VP), thymine, and uracil) and for liquid water for energies between 50 eV and 200 keV. The organic compounds were chosen because experimental optical data were available from the bandgap energy to at least 1 MeV. We were then able to calculate energy-loss functions (ELFs) for each compound and to show that the errors in two ELF sum rules were less than about 10 %. We note that similar ELF

results were obtained by Tahir and Tougaard[12] from reflection electron energy-loss experiments in the survey of optical data available for PMMA and PE.

Two organic compounds that we considered previously[4], bovine plasma albumin and deoxyribonucleic acid, however, were omitted in this study because their ELFs could not determine for energies over 82 eV. We also report new results of IMFP calculations for liquid water with the relativistic FPA and the Boutboul *et al.* approach for energies between 50 eV and 200 keV. Our previous IMFP calculations for water for energies between 50 eV and 30 keV were made with the relativistic FPA but did not consider the effect of the band-gap energy.[7]

2. IMFP Calculations with the Relativistic Full Penn Algorithm

We calculated IMFPs for 14 organic compounds for energies in the 50 eV to 200 keV range with the relativistic full Penn algorithm using the Boutboul *et al.* approach[11] (FPA-BABC) in order to be consistent with our previous IMFP calculations for elemental solids[6] and inorganic compounds.[8] The IMFPs were calculated at equal energy intervals on a logarithmic scale corresponding to increments of 10 % from 3 eV to 1 MeV. We will present IMFPs for energies between 3 eV and 50 eV and between 200 keV and 1 MeV in Figures but these results are of less accuracy and are shown only to illustrate trends.

The relativistic differential cross section (DCS) for inelastic scattering can be written using Hartree atomic units ($m_e = e^2 = \hbar = 1$), where m_e is the electron rest mass, e is the elementary charge, and $\hbar$ is the reduced Planck constant) for energies less than 500 keV,[13] as

$$\frac{d^2\sigma}{d\omega dQ} \approx \frac{1}{v^2} \frac{1+\frac{Q}{c^2}}{Q\left(1+\frac{Q}{2c^2}\right)} \frac{1}{\pi N} \mathrm{Im}\left(\frac{-1}{\varepsilon(Q,\omega)}\right) , \qquad (1)$$

where ω is the energy loss, c is the speed of light, Q is the recoil energy defined by[14]

$$Q\left(Q+2c^2\right)=(cq)^2\,, \tag{2}$$

q is the momentum transfer, N is the number of molecules per unit volume, v is the electron velocity, and Im[$-1/\varepsilon(Q,\omega)$] is the ELF expressed as a function of energy loss ω and recoil energy Q.

We can then write the relativistic DCS as

$$\frac{d^2\sigma}{d\omega dq}\approx\frac{2}{\pi N v^2}\,\mathrm{Im}\left(\frac{-1}{\varepsilon(q,\omega)}\right)\frac{1}{q}, \tag{3}$$

where Im[$-1/\varepsilon(q,\omega)$] is the ELF. In the FPA, the dependence of the ELF on ω can be obtained from the measured ELF for each material (typically from optical experiments) while the dependence of the ELF on q can be obtained from the Lindhard[15] model dielectric function.

The ELF in Equation 3 can be expressed using the full Penn algorithm as

$$\mathrm{Im}\left[\frac{-1}{\varepsilon(q,\omega)}\right]=\int_0^\infty d\omega_p\, g\left(\omega_p\right)\,\mathrm{Im}\left[\frac{-1}{\varepsilon^L\left(q,\omega;\omega_p\right)}\right] \tag{4}$$

where

$$g(\omega)=\frac{2}{\pi\omega}\,\mathrm{Im}\left[\frac{-1}{\varepsilon(\omega)}\right], \tag{5}$$

ε^L denotes the Lindhard model dielectric function for a free-electron gas with plasmon energy $\omega_p\left(=\sqrt{4\pi n}\right)$, n is the electron density, $g\left(\omega_p\right)$ is a coefficient introduced to satisfy the condition Im[$-1/\varepsilon(q=0,\omega)$] = Im[$-1/\varepsilon(\omega)$], and Im[$-1/\varepsilon(\omega)$] is the optical

energy-loss function. The details of the evaluation of Eq. (4) were given in a previous paper[6].

A total inelastic-scattering cross section for a particular electron energy T can be obtained from double integrations of Eq. (3) and use of Eqs. (4) and (5). The corresponding IMFP, λ, can then be computed from $\lambda^{-1} = N\sigma$. The IMFP for an electron energy $T > (E_g + E_v)$, which is measured from the bottom of the valence band for semiconductors and insulators, can be expressed as:[8]

$$\lambda(T)^{-1} = \frac{\left(1+\frac{T-E_g}{c^2}\right)^2}{1+\frac{T-E_g}{2c^2}} \frac{1}{\pi(T-E_g)} \iint_D \frac{1}{q} \mathrm{Im}\left[\frac{-1}{\varepsilon(\omega,q)}\right] dqd\omega \qquad (6)$$

where E_g is the bandgap energy (in hartree) and E_v is the width of the valence band (in hartree) for semiconductors and insulators. The integration domain D is determined from the maximum and minimum energy losses and the largest and smallest kinematically-allowed momentum transfers for a given energy T and ω:

$$D = \left\{(\omega,q) | E_g \le \omega \le \left(T - E_g - E_v\right),\ q_- \le q \le q_+ \right\}, \qquad (7)$$

where

$$q_\pm = \sqrt{(T-E_g)\left(2+(T-E_g)/c^2\right)} \pm \sqrt{\left(T-E_g-\omega\right)\left[2+\left(T-E_g-\omega\right)/c^2\right]} \qquad (8)$$

Table 1 shows the material-property data used in our IMFP calculations and in our analyses of the ELFs and IMFPs. We show values of the molecular weight M, bulk density ρ (g cm^{-3}), number of valence electrons per molecule (N_v), free-electron plasmon energy (E_p), bandgap energy (E_g) in eV, valence-band width (E_v) in eV, and total atomic number (Z) for each compound.

The E_g values were obtained from our previous papers[4] for 26-n-paraffin, adenine, β-carotene, DPHT, guanine, PBS, PMMA, PS, and P2VP. The E_g values for Kapton, PA, and PE were taken from the work of Kumar *et al*.[16], Hüfner[17], and Tanaka[18], respectively. The values of E_g for thymine and uracil were estimated from the ELFs reported by Issacson.[19] The E_g value for water was the median of literature values.[7] The E_v values were estimated from calculations of the valence-band energies with the GAUSSIAN 09 program [20] for 11 molecules (26-n-paraffin, adenine, β-carotene, diphenyl-hexatriene, Kapton, poly(butene-1-sulfone) trimer, polymethylmethacrylate, polystyrene trimer, poly(2-vinylpridine) trimer, thymine, and uracil). For the other three organic compounds (guanine, polyacetylene, and polyethylene), the valence-band energies were estimated from measured valence-band spectra in the literatures.[17,21,22] In the use of GAUSSIAN 09, the initial geometric structures of the organic molecules were optimized with the semiempirical PM7 method.[23] Furthermore, we performed a second optimization of the geometry with the B3LYP/ 6-31 G(d, p) level in the GAUSSIAN 09 program using the Cartesian coordination from the initial optimization of the geometry.

Table 2 shows the sources of optical data for our IMFP calculations. The optical data used for the low-energy region for 12 organic compounds (26-n-paraffin, adenine, β-carotene, DPHT, guanine, Kapton, PA, PBS, PE, PMMA, PS, and P2VP) are the same as for our previous paper.[4] The ELFs for these 12 compounds at higher energy region, typically over 50 eV that was different from compound to compound, were calculated from the atomic scattering factors of Cullen *et al*.[24] The ELF for water between 6.0 eV and 87.0 eV is the same as that used in our previous paper.[7] We used the atomic scattering factors of Cullen *et al*.[24] for energies between 88 eV and 1.12 MeV to determine the ELF for water.

3. Evaluation of the optical energy-loss functions

We checked the internal consistency of our ELF data for each compound with the oscillator-strength or f-sum rule and a limiting form of the Kramers-Kronig integral (or KK-sum rule).[25] The f-sum can be evaluated as the total effective number of electrons per molecule, Z_{eff} , contributing to the inelastic scattering:

$$Z_{\mathrm{eff}} = \left(\frac{2}{\pi\hbar^2\Omega_p^2}\right)\int_{E_g}^{\Delta E_{\max}} \Delta E \,\mathrm{Im}\left[-\frac{1}{\varepsilon(\Delta E)}\right] d(\Delta E), \tag{9}$$

where $\Delta E = \hbar\omega, \Omega_p = \left(4\pi n_a e^2/m\right)^{1/2}, n_a = N_a\rho/M$ is the density of atoms, N_{a} is Avogadro's number, ρ is the mass density, and M is the molecular weight. The maximum energy loss in Equation 9, $\Delta E_{\max}$, was chosen to be 1 MeV. Ideally, the value of Z_{eff} should be equal to (or otherwise close to) the total number of electrons per molecule, Z. The KK-sum can be expressed as:

$$P_{\mathrm{eff}} = \left(\frac{2}{\pi}\right)\int_0^{\Delta E_{\max}} \Delta E^{-1} \,\mathrm{Im}\left[-\frac{1}{\varepsilon(\Delta E)}\right] d(\Delta E) + n^{-2}(0), \tag{10}$$

where $n(0)$ is the limiting value of the refractive index at low photon energies. Table 3 lists the errors in the f-sum and KK-sum rules for each compound, that is, the differences between the computed values of Z_{eff} and P_{eff} and the expected values (the total number of electrons per molecule and unity, respectively).

The RMS errors in the f-sum and KK-sum rules were 4.5 % and 3.0 %, respectively, for our sets of ELF data. The resulting f-sum values are generally superior to the results of our previous work,[4] especially for 26-n-paraffine and β-carotene. The main reason for these differences is associated with the atomic scattering factors used for the ELF calculations in the high-energy region. The atomic scattering factors used here

were obtained from the database of Cullen *et al*.[24] and were taken from Henke *et al*.[26] in the previous work. The reason for the large differences for 26-n-paraffin and β-carotene may be due to the relatively large energy gaps (10 eV for 26-n-paraffin and 6 eV for β-carotene that were missing for photon energies between 40 eV and 50 eV, respectively) in the ELFs used in the previous paper[4], in addition to the above reason. In the present study, we eliminated the energy gaps in the ELFs by using the atomic scattering factors of Cullen *et al*.[24] On the other hand, the errors of the KK-sum rules in Table 3 are not significantly different from our previous results.

The resulting RMS errors (4.5 % for the f-sum error and 3.0 % for the KK-sum error) are comparable to those found in our ELF data sets for our group of 41 elemental solids[5,6] (4.2 % for the f-sum error and 7.7 % for the KK-sum error) and our group 42 inorganic compounds[8] (4.1 % for the f-sum error and 3.5 % for the KK-sum error).

4. Results

4.1 Calculated IMFPs from the relativistic full Penn algorithm with the Boutboul et al. approach

Table 4 shows our calculated IMFPs for the 14 organic compounds and for water from the full Penn algorithm with the Boutboul *et al*.[11] approach (FPA-BABC). The IMFPs in Table 4 are shown as a function of the electron kinetic energy E with respect to the bottom of the conduction band between 50 eV and 200 keV; i.e., $E = T - E_g - E_v$. Plots of IMFPs as a function of electron energy are shown as solid circles in Figs. 1 to 4. IMFPs are included in these plots for energies less than 50 eV and over 200 keV to illustrate trends. The IMFPs for energies less than 50 eV, however, are not considered as reliable as those at higher energies[2, 5] while the calculated IMFPs for energies larger than 200 keV

must be slightly larger than the correct values because we neglected the contribution of the transverse term in the DCS .[6]

The plots of calculated IMFPs in Figs. 1 to 4 show similar dependences on electron energy for energies over 100 eV for all of the compounds. For energies less than 30 eV, however, there are appreciable variations in the shapes of the plots that are mainly due to the different bandgap energies and different shapes of the ELFs for each material. We will describe these effects in the following two subsections.

4.2 Comparison of new IMFPs with our previous results

Figure 5 shows plots of the ratios of IMFPs in Table 4 for 12 organic compounds that were obtained with the FPA-BABC algorithm (λ_{new}) to the corresponding IMFPs that we published previously[4] (λ_{old}). The differences from unity in Fig. 5 are due mainly to differences in the optical ELFs as stated in Section 3 and to differences in the algorithms used for the IMFP calculations (FPA and FPA-BABC).

The ratios for the 12 compounds in the Fig. 5 are within ± 6 % of unity for energies between 50 eV and 2000 eV except for polyethylene for which the ratios are between 1.06 and 1.07 for energies between 50 eV and 90 eV. On the other hand, we see large increases of the ratios for energies less than 30 eV for polyethylene (E_g = 7.35 eV), 26-n-paraffin (E_g = 6.0 eV), PBS (E_g = 6.0 eV), and PMMA (E_g = 5.0 eV). We also see a small decrease of the ratio for energies less than 30 eV for guanine.

The varying magnitudes of the ratios in Fig. 5 for energies less than 30 eV are mainly associated with our use of the Boutboul *et al.*[11] algorithm for our new IMFP calculations and specifically to the inclusion of the bandgap energy in Eqns. (6) to (8). In our previous calculations of IMFPs for organic compounds,[4] we did not consider the effect

of the bandgap energy. We also assumed that the Fermi energies of each compound were 15 eV but we now find that the valence-band widths of the 14 compounds in Table 1 vary between 12.9 eV (for thymine) to 18.8 eV (for Kapton). Thus, the maximum excitation energy (corresponding to the upper limit of the ω integral, $\Delta E_{\max}$ in Eq. (6)) was $T - E_f$ in our previous calculations and the minimum excitation energy was zero. In the present calculations, the upper limit of the ω integral ensures that an incident electron will always have sufficient energy to remain in the conduction band. The upper limit is then given by $\Delta E_{\max} = T - E_v - E_g$ [$= T - E_f - (E_g/2)$]. The minimum excitation energy or the lower limit of the ω integral corresponds to the E_g values. The IMFP values of compounds that have relatively large bandgap energies (such as polyethylene and 26-n-paraffin) will therefore be larger than those in our previous paper (as shown in Fig. 5) due to the decrease in the domain D for the ω (or energy) integral as given in Eq. (7).

4.3 Dependence of IMFPs on electron energy

In previous work [6,7,8], we analyzed the dependence of the calculated IMFPs for each material on electron energy with a modified form of the Bethe equation for inelastic-electron scattering in matter.[10] The relativistic form of the modified Bethe equation can be described approximately as:[6]

$$\lambda(E) = \frac{\alpha(E)E}{E_p^2\left\{\beta[\ln(\gamma\alpha(E)E)] - (C/E) + \left(D/E^2\right)\right\}}, \quad \text{(nm)} \qquad (11)$$

where

$$\alpha(E) = \frac{1 + \frac{E}{\left(2m_e c^2\right)}}{\left[1 + \frac{E}{\left(m_e c^2\right)}\right]^2} \approx \frac{1 + \frac{E}{1021999.8}}{(1 + E/510998.9)^2}\ , \qquad (12)$$

$$E_{\mathrm{p}} = 28.816 \left(\frac{N_{\mathrm{v}} \rho}{M} \right)^{0.5}, \qquad \text{(eV)} \tag{13}$$

and E is the electron kinetic energy (in eV) above the bottom of the conduction band (= $T - E_{\mathrm{v}} - E_{\mathrm{g}}$), ρ is the bulk density (in g cm^{-3}), N_{v} is the number of valence electrons per atom or molecule, and β, γ, C, and D are parameters. Satisfactory fits were made with Eqs. (11)- (13) to the calculated IMFPs for the 14 organic compounds and liquid water for energies between 50 eV and 200 keV, as shown by the solid lines in Figs. 1 to 4, and the values of β, γ, C, and D from each fit are shown in Table 5.

The quality of each fit was assessed from the root-mean-square percentage difference, RMS:

$$\mathrm{RMS} = 100 \times \left[\sum_{i=1}^{n} \left(\frac{\lambda_{fit}(E_i) - \lambda(E_i)}{\lambda(E_i)} \right)^2 / n \right]^{0.5}, (\%) \tag{14}$$

where $n = 83$ is the number of electron energies in Table 4. Values of RMS for each solid are shown in Table 5. These values range from 0.12 % to 0.27 % while the average value of RMS for the 15 compounds was 0.17%. This average value of RMS is much smaller than the average values found in similar fits for our group of 41 elemental solids (0.68 %)[6] and 42 inorganic compounds (0.60 %).[8] Equations (11)-(13) are thus convenient analytical representations of the calculated IMFPs (e.g., for interpolation).

We also see large differences in the energy dependences of IMFPs for each compound for energies less than 30 eV as shown in Figs. 1 – 4. In the previous subsections, we pointed out that the value of the bandgap energy E_{g} and the shapes of ELFs are important in determining the magnitudes of IMFPs for nonconductors at energies less than 30 eV. To obtain more insight, we investigated the effects of different E_{g} values on the calculated IMFPs of PA, PE, and PS. We chose these compounds as representative materials because one compound (PE) has a relatively large E_{g} value (7.35 eV) and a

strong energy-loss peak at around 4.5 eV, another (PS) has an intermediate E_g value (6.0 eV) and no obvious loss peak less than 10 eV, and the other (PA) has a small E_g value (1.38 eV) and a sharp peak at 7 eV. The ELFs of these three compounds are shown in Fig. 6.

Figure 7 shows IMFPs calculated from the optical ELFs of polyacetylene, polyethylene, and polystyrene with the FPA-BABC algorithm as a function of electron energy from 3 eV to 100 eV with both the actual E_g values for each compound (solid circles) and with E_g set equal to zero (solid lines). Figure 7 indicates that inclusion of the bandgap energy in the IMFP calculation generally leads to IMFP increases for $E < 30$ eV. This increase is due to the decrease in the ω (or energy) integral domain D as given by Equation 7. The lower limit of the ω integral, ΔE_{min}, is set equal to the bandgap energy for nonconductors. This lower limit corresponds to the minimum excitation energy for electrons in the material. The maximum excitation energy corresponds to the upper limit of the ω integral, ΔE_{max}.

If we ignore for the moment the effect of E_g, the magnitudes of the IMFPs for energies less than 30 eV can be explained by differences in the shapes of the ELFs, in particular the presence or absence of a peak below 10 eV. For example, we see that the IMFPs for PA with $E_g = 0$ in Fig. 7 are much smaller than the IMFPs for PE and PS with $E_g = 0$ especially for energies less than 10 eV. This result must be due to the existence of the strong energy-loss peak at around 4.5 eV for PA as shown in Fig. 6. On the other hand, the IMFPs for PE with $E_g = 0$ are generally the same as the IMFPs for PS with $E_g = 0$ for energies between 20 eV and 100 eV, but we see that the IMFPs of PE are slightly larger than the IMFPs of PS for energies between 7 eV and 20 eV due to the existence of the sharp energy-loss peak at about 7 eV for PS (the $\pi \rightarrow \pi^*$ transition) in Fig. 6. Nevertheless,

the energy dependences of the IMFPs for energies less than 30 eV are dominated by the magnitude of E_g, as shown in Fig. 7.

4.4 Comparison of calculated IMFPs with IMFPs from the relativistic TPP-2M equation

We developed a relativistic version of our earlier predictive IMFP formula,[4] designated as the relativistic TPP-2M equation, to estimate IMFPs in materials for electron energies between 50 eV and 200 keV.[6] Our original non-relativistic TPP-2M equation was developed from an analysis of our calculated IMFPs for a group of 27 elemental solids[2] and a group of 14 organic compounds[4] for electron energies between 50 eV and 2 keV. The relativistic TPP-2M formula is based on Eqs. (11) – (13), and the following expressions for the material-dependent parameters in this equation:[6]

$$\beta = -1.0 + \frac{9.44}{\left(E_p^2 + E_g^2\right)^{0.5}} + 0.69\rho^{0.1} \quad (\mathrm{eV^{-1}nm^{-1}}) \tag{15a}$$

$$\gamma = 0.191\rho^{-0.5} \qquad (\mathrm{eV^{-1}}) \tag{15b}$$

$$C = 19.7 - 9.1U \qquad (\mathrm{nm^{-1}}) \tag{15c}$$

$$D = 534 - 208U \qquad (\mathrm{eV\ nm^{-1}}) \tag{15d}$$

$$U = \frac{N_v\rho}{M} = \left(\frac{E_p}{28.816}\right)^2 \tag{15e}$$

where the bandgap energy E_g is in eV. Equations (15) are the same expressions as those developed earlier for our non-relativistic TPP-2M equation.[4]

IMFPs calculated from the relativistic TPP-2M equation for our 15 compounds are shown in Figs. 1 to 4 as dashed lines, and Table 6 shows values of the RMS deviations

between these IMFPs and the IMFPs calculated from optical data shown in Table 4. The average RMS deviation for the 15 compounds over the 50 eV to 200 keV range is 7.2 %. This average deviation is less than those found in similar comparisons for our group of 41 elemental solids (11.9 %)[6] and for our group of 42 inorganic compounds (10.7 %)[8] for the same energy range.

Figure 8 shows plots of ratios of IMFPs calculated from the relativistic TPP-2M equation [Eqs. (11), (12), (13) and (15)] to IMFPs calculated from optical data for the 14 organic compounds and for liquid water (shown in red) as a function of electron energy in order to assess visually the reliability of the TPP-2M equation for energies up to 200 keV. Ideally, these ratios should not change with energy and should be close to unity. The ratios in Fig. 8 for each compound are nearly constant for energies between about 300 eV and 200 keV (the relative deviations are less than 3 %) but there are often substantial changes at lower energies (typically for energies less than about 200 eV).

We see relatively large values of the ratios in Fig. 8 for polyacetylene (ratios > 1.1 for energies over 300 eV) and relatively small values for diphenyl-hexatriene (ratios < 0.9 for all energies). For energies over 300 eV, the ratios for each compound do not vary appreciably with electron energy. Except for PA and DPHT, the ratios are within about 10 % from unity for energies between 300 eV and 200 keV. The averages of the ratios are 0.99 ± 0.07 and 1.00 ± 0.07 for maximum energies of 992.3 eV and 9897.1 eV, respectively. We conclude that the relativistic TPP-2M formula is useful for estimating IMFPs in solid materials for energies between 50 eV and 200 keV although the accuracy of these estimates is likely to be poorer for energies less than about 200 eV.

4.5 Effect of damping on IMFP calculations with the full Penn algorithm

The Lindhard dielectric function provides the q-dependence for the ELF $[\varepsilon(q,\omega)]$ in IMFP calculations with the full Penn algorithm. However, the Lindhard ELF does not have a damping term. Several authors have pointed out the importance of including a damping factor in calculations of IMFPs since damping must be necessary due to the finite plasmon lifetime in real materials.[27,28,29] We will therefore compare our IMFPs at electron energies between 5 eV or 10 eV and 2000 eV to the IMFPs that were calculated with the Mermin-Penn algorithm[29] ,which includes the plasmon damping term, using the approach of Boutboul *et al.* (same as our FPA-BABC calculations).

In the Mermin-Penn algorithm, the ELF in Equation 3 must be replaced by

$$\mathrm{Im}\left[\frac{-1}{\varepsilon(q,\omega)}\right] = \int_0^\infty d\omega_p\, G(\omega_p)\,\mathrm{Im}\left[\frac{-1}{\varepsilon^M(q,\omega;\omega_p)}\right], \tag{16}$$

where

$$G(\omega) = \frac{2}{\pi\omega^2\gamma_D}\mathrm{Im}\left[\frac{-1}{\varepsilon(\omega)}\right]\sqrt{2\omega\left(\omega^2+{\gamma_D}^2\right)\left(\sqrt{\omega^2+{\gamma_D}^2}-\omega\right)}, \tag{17}$$

γ_D is the damping coefficient, and ε^M is the Mermin dielectric function that is given by

$$\varepsilon^M(q,\omega) = 1 + \frac{(1+\mathrm{i}\gamma_D/\omega)\left[\varepsilon^L(q,\omega+\mathrm{i}\gamma_D)-1\right]}{1+(\mathrm{i}\gamma_D/\omega)\left[\varepsilon^L(q,\omega+\mathrm{i}\gamma_D)-1\right]/\left[\varepsilon^L(q,0)-1\right]}. \tag{18}$$

We investigated the influence of the damping coefficient on the calculated IMFPs for two selected compounds, guanine, and water. IMFPs for these compounds were calculated using the non-relativistic Mermin-Penn-BABC approach with selected values of the damping coefficient (0.2 eV, 1 eV, 1.5 eV, 2 eV, and 5 eV) for electron energies between 5 eV and 2000 eV. We wished to determine how the calculated IMFPs varied with damping

coefficient over a plausible range of this parameter. We also note that damping coefficients of 1.5 eV for Al and 2 eV for Au improved the agreement between calculated and measured IMFPs for electron energies between 5 eV and 10 eV.[29]

Figures 9A and 9C show IMFPs calculated from optical ELFs by the Mermin-Penn-BABC (M-P-BABC) approach for guanine and water using the chosen values of the damping coefficient as a function of electron energy from 5 eV to 2 keV for guanine in Fig. 9A and from 10 eV to 2 keV in Fig. 9C for water. The solid lines in Figs. 9A and 9C are our calculated IMFPs from the FPA-BABC algorithm shown in Table 4. Figures 9B and 9D shows ratios of IMFPs from the M-P approach to those from the FPA algorithm for guanine (Fig. 9B) and water (Fig. 9D) as a function of electron energy.

Figure 9A and 9C show that IMFPs from the Mermin-Penn-BABC approach for guanine and water are generally in good agreement with the FPA-BABC IMFPs for electron energies between 50 eV and 2 keV. We also see the IMFP ratios in Figs. 9B and 9D increase as the value of γ_D increases for energies above about 50 eV. For energies below 50 eV, the opposite trend is observed.

When the value of γ_D is 0.2 eV, the M-P IMFPs in Fig. 9 are in excellent agreement with the FPA IMFPs. The maximum difference between the M-P and FPA IMFPs are less than 1 % when $\gamma_D = 0.2$ eV. The average differences are less than 3 % when $\gamma_D \leq 2.0$ eV for both materials. For $\gamma_D = 5.0$ eV, the IMFP ratios for guanine and water increase to 1.07 and 1.08 at 2 keV, respectively. On the other hand, for energies less than 50 eV, the IMFP ratios in Figs. 9B and 9D decrease rapidly as the value of γ_D increases. For example, the ratio decreases to 0.7 for water at an energy of 50 eV. Since our FPA IMFPs are less reliable at energies below 50 eV, as mentioned in Section 4.1, compared to the IMFPs for higher energies, the IMFP ratios shown in Figs. 9B and 9D should be considered only as guides.

We also point out that the effect of E_g is large on the IMFPs calculated from the FPA for energies less than 50 eV, as shown in Fig. 7. That is, uncertainty in the bandgap energy can have a large effect on the IMFP. The electron exchange effect is also important in this energy region, as will be discussed in the next Section.

We conclude that the effect of plasmon damping on IMFPs calculations with the FPA-BABC algorithm is generally small (< 3 %) for energies over 50 eV even for the materials that have damping coefficients as large as for Au (γ_D = 2.0 eV).

5. Discussion

We will now make comparisons of our calculated IMFPs for organic compounds and water with other IMFP calculations and with IMFP measurements from elastic-peak electron spectroscopy (EPES), from photoemission experiments, and from experiments in which electrons were transmitted through thin films or nanoparticles. We will mainly make comparisons with calculated and measured IMFP values that had not been published at the time of our previous works.[4,7] Although IMFP calculations from the present relativistic FPA-BABC algorithm are expected to provide only a qualitative guide for energies less than 50 eV, we show our calculated IMFPs for these low energies in Figs. 10 and 11 to make comparisons with other IMFP results.

5.1 Comparison of our inelastic mean free paths with other calculated inelastic mean free paths

Figure 10 shows comparisons of our calculated IMFPs for 14 organic compounds and water with other calculated IMFPs for energies between 5 eV and 10 keV.

We have plotted the literature IMFP data in Fig. 10 without any energy-scaling corrections. That is, our IMFPs are shown as a function of energy above the bottom of the conduction band and the literature IMFPs are shown as they were reported. We have thus assumed that these IMFPs were also determined as a function of energy above the bottom of the conduction band even if this was not stated in the original papers.

Akkerman and Akkerman[30] calculated IMFPs for 10 organic compounds (26-n-paraffin, β-carotene, diphenyl-hexatriene or DHT, guanine, polyacetylene, poly(butene-1-sulfone) or PBS, polyethylene, PMMA, polystyrene, poly(2-vinylpridine) or P2VP) for energies from 20 eV to 10 keV using a dielectric model with a quadratic dispersion equation. They fitted Drude functions to the optical ELFs for valence-electron excitations and made separate IMFP calculations for core-electron excitations using an atomic model. Total IMFPs for their 10 organic compounds were reported with and without a correction for the effects of electron exchange (XC) that was based on Ashley's expression.[31]

Figures 10(A) to 10(F) show comparisons of our IMFPs with the IMFPs of Akkerman *et al*. for their 10 compounds. The IMFPs of Akkerman *et al*. both with and without XC for 26-n-paraffin in Fig. 10(A) are in good agreement with our IMFPs for energies between 100 eV and 10 keV, with RMS differences of 6.6 % and 5.1 %, respectively. At lower energies, however, there are increasing differences between their IMFPs and our IMFPs. Our smaller IMFPs in this energy region compared to the IMFPs of Akkerman *et al*. without XC are likely due to the contributions of single-electron excitation to the ELF, which were neglected in their algorithm. The IMFPs of Akkerman et al. with XC, are even larger typically for energies under 100 eV because of the indistinguishability between incident and scattered electrons which reduces the energy range in the integral for energy loss. Similar trends were found in the comparison with

the Akkerman *et al.* IMFPs for PMMA in Fig. 10(E). Their IMFPs with and without XC are in good agreement with our IMFPs for energies between 100 eV and 10 keV, with RMS differences of 8.7 % and 6.2 %, respectively. For β-carotene, DMHT, guanine, PBS, polyethylene, polystyrene and P2VP, we see excellent agreements between the Akkerman *et al.* IMFPs without XC and our IMFPs for energies over 100 eV with RMS differences of less than 6 % for energies between 100 eV and 10 keV for seven compounds: β-carotene: 2.8 %; DMHT: 3.4 %; guanine: 5.4 %; PBS: 5.5%; polyethylene: 4.3 %; polystyrene: 3.2 %; and P2VP: 3.1 %. On the other hand, the Akkerman *et al*. IMFPs with XC are larger than our IMFPs by about 10 % between 100 eV and 10 keV. This difference is mainly due to electron exchange effect especially for energies over 300 eV rather than the reduction of the integrated energy range for energy loss that attributed to the electron indistinguishability.

We note that the comparisons of IMFPs with and without exchange correction and with the choice of ω_{Emax} for energy loss were already discussed in our previous papers [5,7] for elemental solids and water. Powell and Jablonski[32] also reported the effect of electron exchange correction on IMFPs. In general, exchange of energetic electron would increase IMFPs by between about 10 and 15% for election energies between 50 and 100 eV.[32] The choice of maximum energy loss $\omega_{Emax} = T/2$ increases IMFP values from the FPA by up to about 50% to around 50 eV compared with IMFPs with $\omega_{Emax} = T - E_f$.[7]

For polyacetylene, the IMFPs of Akkerman *et al.* with and without XC are clearly larger than our IMFPs for energies between 20 eV and 10 keV. Our IMFPs at 100 eV and 1000 eV are smaller than the Akkerman *et al*. IMFPs without XC by 12 % and 18 %, respectively, while the differences at these energies for the Akkerman *et al.* IMFPs

with XC are 35 % and 24 %, respectively. The main reason for these differences is that different ELFs were used in the IMFP calculations for polyacetylene. The value of Z_{eff} for the Akkerman *et al*. ELF was 13.7, which is smaller than our Z_{eff} value of 15.26, as shown in Table 3.

Tan *et al*[33] reported total cross sections for inelastic scattering of electrons in five bases: guanine, adenine, thymine, cytosine, and uracil for energies between 20 eV and 10 keV using dielectric response theory and the Penn simplified single-pole approximation (with a quadratic dispersion equation for q) and the Born-Ochkur electron-exchange correction.[34,35] They also used an empirical approach to obtain ELFs for organic compounds without available optical data. They assumed that the optical ELFs could be represented by a single Drude function with parameters described by the mean atomic number.

Figure 10 show comparison of our IMFPs with the IMFPs of Tan *et al*. for adenine (in Fig. 10(A)), guanine (in Fig. 10(C)), thymine (in Fig. 10(G)), and uracil (in Fig. 10(G)). Their IMFPs for these compounds are substantially larger than our IMFPs for energies less than 50 eV. These differences are similar to those found in the comparisons of our IMFPs with the IMFPs of Akkerman *et al*. with XC. The fact that our IMFPs in this energy region are less than those of Tan *et al.* is likely due to the contribution of single-electron excitations to the ELF that were neglected in the single-pole approximation used by Tan *et al.* As discussed above, Tan *et al.* included exchange in their calculations which reduces the integration range for energy loss due to the indistinguishability of incident and scattered electrons. The IMFPs of Tan *et al.* for adenine, guanine, and thymine are in good agreement with our IMFPs for energies between 200 eV and 10 keV where the RMS differences are 3.4 %, 2.2 %, and 4.8 %,

respectively. For uracil in Fig. 9(G), we see that the IMFPs of Tan *et al.* are larger than our IMFPs by about 10 % in the same energy range. Although the cause of this difference is unknown, we believe it is probably due to differences in the ELFs used for each IMFP calculation.

In 2011, de Vera *et al.*[36] reported IMFPs and stopping powers for electrons, protons and α-particles for four organic polymers : PMMA, Kapton, polyacetylene, and P2VP for electron energies between 10 eV and 10 keV. They used the dielectric formalism for the calculations of electron IMFPs together with the Mermin energy-loss function – generalized oscillator strength (MELF-GOS) method. They also applied the Born-Ochkur approximation to take account of electron exchange between the incident electron and the target electrons.

Figure 10 shows comparisons of our IMFPs with the IMFPs of de Vera *et al.* for Kapton (in Fig. 10(C)), polyacetylene (in Fig. 10(D)), PMMA (in Fig. 10(E)), and P2VP (in Fig. 10(F)). For Kapton, polyacetylene, and P2VP, our IMFPs are in excellent agreement with the IMFPs of de Vera *et al.* for energies between 100 eV and 10 keV, where the RMS differences are 6%, 2 %, and 4%, respectively. Their IMFPs are larger than our IMFPs between 20 eV and 100 eV due to the contribution of exchange in their algorithm. For energies between 10 and 20 eV, we see good agreements between our IMFPs and their IMFPs. This agreement is probably due to the fact that, in this energy range, the upper limit of the de Vera *et al.* energy integral is roughly the same as the upper limit of the energy integral in our FPA-BABC algorithm.

On the other hand, the IMFPs of de Vera *et al.* for PMMA are about 20 % smaller than our IMFPs for energies between 100 eV and 10 keV. We also see larger differences between our PMMA IMFPs and the de Vera *et al.* IMFPs for energies less than 20 eV

compared to the results for the three other polymers. The reason for these results is that the ELFs used in the two IMFP calculations must have been different. The details are unclear, but the IMFP differences may be due to the fact that, below about 100 eV, de Vera *et al.* approximated the ELF with Drude functions while above 100 eV the ELF was calculated with a hydrogenic GOS model. In our work with the FPA-BABC algorithm, we used measured ELFs for direct calculations without approximating them with functions as shown in Eqs. (4) and (5).

Garcia-Molina *et al.*[37] reported IMFP calculations for DNA, protein, lipid, carotene, sugar as well as liquid water and ice for electron energies between 10 eV and 10 keV. These IMFPs were calculated using the dielectric formalism with a Mermin energy loss function and a generalized oscillator strength model to determine the ELFs of these materials for arbitrary energy and momentum transfers using electron energy-loss spectroscopy data as input. The ELFs for the organic compounds at zero momentum transfer were obtained from measured electron energy-loss spectra in the transmission electron microscope (TEM) for energy losses up to 30 eV.[38]

Figure 10(B) shows comparisons of our IMFPs with the IMFPs of Garcia-Molina *et al.* for β-carotene for energies between 10 eV and 10 keV. We see similar differences between the Garcia-Molina *et al*. IMFPs and our IMFPs for energies between 20 eV and 100 eV as the differences found between the IMFPs of de Vera *et al*.[36] and our IMFPs for Kapton (Fig. 10(C)), PA (Fig. 10(D)), and P2VP (Fig. 10(F)) because similar algorithms were used for both IMFP calculations. However, the IMFPs of Garcia-Molina *et al.* are larger than our IMFPs by about 15 % for energies over 200 eV. These IMFP differences must be due to the use of different ELFs in each calculation.

Figure 10(H) shows comparison of our IMFPs for water with IMFPs calculated by Garcia-Molina *et al.*[37], Emfietzoglou *et al.*[39], Nguyen-Truong,[40] and Flores-Mancera *et al.*[41] together with the IMFPs calculated from the FPA with E_g = 0 eV for energies between 10 eV and 10 keV. We see that our IMFPs are in generally good agreement with the other IMFPs for energies between 300 eV and 10 keV. For energies less than 30 eV, the energy dependence of our IMFPs is similar to the other results in Fig. 10(H) except for the energy dependence of the IMFPs of Nguyen-Truong. As we pointed out previously,[8] the value of E_g has a significant effect on IMFPs from the FPA algorithm in this low-energy region. As shown in Fig. 10(H), IMFPs from the FPA-BABC algorithm with E_g = 7.9 eV (solid line) are systematically larger than those from the FPA algorithm with E_g = 0 (dashed line) for energies less than about 70 eV due to the decrease in the ω integral domain (Eq. (7)). However, it is hard to compare the differences IMFPs from different publications in more detail for energies less than 30 eV because of likely differences in the energy scales, i.e., the positions of zero on each energy scale, which would have a large impact in this energy region. For energies between 30 eV and 300 eV, the IMFPs from different groups are different. These different energy dependences must be due mainly due to differences in the algorithms for each calculation and to the choice of whether or not to include a correction for electron exchange. We will now make more detailed comparisons for each set of calculated IMFPs.

Garcia-Molina *et al.*[37] published IMFPs for liquid water, ice, and several biological materials in 2017 for energies between 10 eV and 10 keV. The ELF for water at zero momentum transfer was obtained from the experimental data of Hayashi *et al.*[42] and was fitted with three Drude functions to represent valence-electron excitations. They calculated IMFPs for water from this optical ELF with the MELF-GOS model and

included the Born-Ochkur electron-exchange correction.[43] Their energy integration range was from 0 to Min[$(T + E_g)/2$, $T - E_f$] for outer-shell electron excitations. They used E_g = 7 eV and E_f = 4 eV. Figure 10(H) shows excellent agreement of their IMFPs with our IMFPs for energies between 200 eV and 10 keV with an RMS difference of 1.6 %. For energies between 14 eV and 200 eV, the Garcia-Molina *et al*. IMFPs are larger than our IMFPs by between 1 % and 34 %. This result is mainly due to the decrease in their integration range for energy loss [$0 \leqq \omega \leqq (T + E_g)/2$] due to electron indistinguishability used in the Born-Ochkur electron-exchange approximation compared to our integration range for energy loss shown in Eq. (7). We also point out that their value for the Fermi energy (4 eV) is appreciably smaller than our value (14 eV). This difference probably affects the energy dependence of the IMFP for energies less than 40 eV. If we use E_f = 4 eV in the calculations of IMFPs with the FPA-BABC approach, the ratios of the Garcia-Molina *et al*. IMFPs to the IMFPs found with E_f = 4 eV are between 0.93 and 1.84 for energies between 12 eV and 40 eV. The RMS difference between them is 31 %, which is smaller than the RMS value of 47 % found from our calculations with E_f =14 eV.

Emfietzoglou *et al.*[39] reported calculations of inelastic cross sections or IMFPs for liquid water for energies from 10 eV to 10 keV in 2017 that were calculated with the Emfietzoglou-Cucinotta-Nikjoo (ECN) model and with the ECN model modified by corrections to the first-Born approximation. For their calculations with the ECN model, Emfietzoglou *et al.* fitted the imaginary part of the dielectric function ε_2 (instead of the ELF) from the experimental data of Hayashi *et al*.[42] These fits were made with four Drude functions and five derivative Drude functions to represent outer-shell electronic transitions. They also used empirical dispersion equations at $q \neq 0$ for energy and lifetime broadening that were deduced from their fit to the inelastic-scattering X-ray

spectroscopy (IXSS) data of Hayashi *et al.* We show the calculated IMFPs from the ECN model in Fig. 10 (H) as solid triangles. These IMFPs are in excellent agreement with our IMFPs for energies between 100 eV and 10 keV, with an RMS difference of about 4 %. In our previous paper[7] that reported IMFPs for water, we pointed out that values of the static structure factor $S(q)$[44] that was calculated from the optical ELF with FPA were in excellent agreement with those derived from the IXSS experiments of Hayashi *et al.* between q = 0.69 atomic units and q = 3.59 atomic units. Since Emfietzoglou *et al.* determined empirical dispersion relations from the same IXSS data, the ECN model must give essentially the same $S(q)$ values that were calculated from the FPA. This result means that the q-dependence of the ELFs in each algorithm should be in reasonable agreement with each other in the range $0.69 \leq q \leq 3.59$ in atomic units. We therefore expect that the IMFPs from the FPA and ECN approaches should be in generally good agreement for energies over 100 eV, as seen in Fig. 10(H). We also see that the ECN IMFPs are larger than the FPA IMFPs by between 6 % and 10 % for energies between 30 eV and 80 eV. This result must be due mainly to the different values for the maximum energy loss used in each IMFP calculation.

In the corrected ECN model of Emfietzoglou *et al*.,[34] the total inelastic-scattering cross section was the sum of three terms; the first order Born-approximation term, the second-order correction term from Ashley's soft-collision approximation,[45] and the exchange term that was calculated from the non-relativistic Moller formula.[46] Figure 10(H) shows the IMFPs obtained from this corrected ECN approach. These IMFPs are larger than our IMFPs for energies between 20 eV and 10 keV. For energies over 500 eV, the corrected-ECN IMFPs are larger than our IMFPs by between 5 % and 10 %, and the RMS difference is 6 %. On the other hand, the corrected-ECN IMFPs are larger than our

IMFPs by between 15 % and 67 % for energies between 30 eV and 300 eV. We believe that this difference is mainly due to the inclusion of the electron-exchange term in the corrected-ECN approach.

Nguyen-Truong[40] calculated IMFPs for water and energies between 1 eV and 10 keV with the Mermin-Penn algorithm (MPA) and the Mermin form of the Levine-Louie dielectric function that included the correction for the band-gap effect on the Lindhard ELF. He also adopted the Born-Ochkur exchange correction. The maximum energy loss is then given by $\omega_{max} = \left(T + E_g\right)/2$ due to the indistinguishability between the primary and secondary electrons. His calculated IMFPs are shown in Fig. 10(H) as solid squares. These IMFPs are in excellent agreement with our IMFPs for energies between 300 eV and 10 keV, with an RMS difference of about 2 %. On the other hand, the Nguyen-Truong IMFPs are larger than our IMFPs for energies between 40 eV and 270 eV by between 7 % and 20 %. These differences are mainly due to the Born-Ochkur exchange correction and to the maximum energy loss for his model ($\omega_{max} = \left(T + E_g\right)/2$) being smaller than our maximum energy loss ($\omega_{max} = T - E_{\mathrm{g}} - E_{\mathrm{v}}$) in this energy region. We also see a quite different energy dependence of his IMFPs for energies less than 40 eV compared to our IMFPs. This result must be mainly due to the fact that the maximum energy loss in this energy range in his work is larger than our maximum energy loss for energies less than 40 eV ($\approx 3E_{\mathrm{g}} + 2E_{\mathrm{v}}$). Therefore, as shown in Figure 10(H), the Nguyen-Truong IMFPs are smaller than our IMFPs for energies less than 30 eV.

Flores-Mancera *et al.*[41] calculated IMFPs for water and energies between 10 eV and 433 keV with the relativistic FPA-BABC algorithm (the same algorithm that we used for our calculations). Their resulting IMFPs are shown in Fig. 10(H) as solid diamonds. The Flores-Mancera *et al*. IMFPs are in excellent agreement with our IMFPs for energies

between 20 eV and 10 keV, with an RMS difference of about 2 %. For energies over 200 eV, the Flores-Mancera *et al*. IMFPs are always larger than our IMFPs by between 2 % and 3 %. This result must be due mainly to differences in the ELFs for each calculation.[41] On the other hand, we see that the Flores-Mancera *et al*. IMFPs are smaller than our IMFPs for energies between 10 eV and 20 eV. A similar result occurs with IMFPs calculated from the FPA with $E_g = 0$, as shown by the dashed line in Fig. 10(H). The differences between their IMFPs and our IMFP at low energies must be due to the different minimum energy-loss values used in each calculation. They set ω_{min} as the first energy loss above mid-gap where the ELF exceeds a threshold of 10^{-5} instead of E_g in order to include excitonic excitations.

5.2 Comparison of our inelastic mean free paths with measured inelastic mean free paths

There are few IMFP measurements for organic compounds. Use of the EPES technique is generally difficult due to the likelihood of sample damage caused by the incident electron beam. Measurements of effective attenuation lengths (EALs) by X-ray photoelectron spectroscopy are also difficult [47] although we did report some EAL measurements for water in a previous paper.[7] There are predictive formulas for determining EALs from IMFPs, as described in the above reference 47. These predictive formulas [e.g., Eq. (20)[47]] can be used "in reverse" to estimate IMFPs from EALs if one can make an initial estimate of the IMFP in order to determine the single-scattering albedo.

Substantial progress in determining IMFPs for liquid water has been made in recent years through the development of photoelectron spectroscopy of water microjets[48] and droplet photoelectron imaging.[49] We will make comparisons in this Section of our

calculated IMFPs with values that have been obtained from a number of experimental techniques. The comparisons for water will supplement those presented in our previous paper.[7]

Figure 11(A) shows a comparison of our IMFPs for PA with IMFPs from EPES experiments for energies between 200 eV and 5 keV.[50,51] The measured density of PA in the Lesiak *et al*.[50] experiments was 1.36 g cm^{-3} which is appreciably higher than our value (1.13 g cm^{-3}). This density difference could affect the IMFP values. In addition, XPS measurements showed appreciable amounts of contamination in their PA samples (mainly O and Si) resulting from their synthesis of PA. There is also the possibility of a density distribution with depth in their PA samples that could affect the energy dependence of the measured IMFPs.[50]

Gergely *et al.*[51] also reported IMFPs for PA and for energies between 400 eV and 2000 eV from EPES experiments with the same PA samples as those used by Lesiak *et al.* They applied a surface-excitation correction (SEC) to the measured elastic-peak intensities using the Chen formula[52] but this correction did not make an appreciable change to their IMFP values, as shown in Fig. 11(A). It is, however, difficult to make surface-effect corrections for materials with different electronic properties (PA and their reference materials, Ni and Ag)

While the IMFPs of Lesiak *et al*. and Gergely *et al*. in Fig. 11(A) are of similar magnitude to our calculated IMFPs, they show a much stronger dependence on electron energy. For energies less than about 400 eV, the IMFPs of Lesiak *et al*. are smaller than our calculated IMFPs while for energies above about 1.5 keV, the IMFPs of Lesiak *et al*. and Gergely *et al*. are larger than our IMFPs. These differences are believed to be due to density and composition differences with depth in the PA samples associated with sample

preparation and/or to chemical changes induced by electron bombardment in the EPES experiments.[53]

Figure 11(B) shows a comparison of our IMFPs for PS with IMFPs measured by transmission electron energy-loss spectroscopy and by TEM for energies at 20 keV, 120 keV, and 200 keV.[54,55] Swanson and Powell reported IMFPs and inelastic-scattering cross sections associated with the dominant 21 eV energy loss of 20 keV electrons transmitted thorough 120 nm and 162 nm films of polystyrene in 1966.[54] These IMFPs were determined using a comparison method in which intensities of the 21 eV loss in a PS film and of the 15 eV loss in an Al film at zero scattering angle were compared in consecutive measurements. The IMFP for the 15 eV energy loss in Al had been determined in separate experiments and a model calculation was used to account for the angular distributions of loss intensities that were not measured in the comparison experiments. The average value of the IMFP for the 21 eV loss in PS was then found to be 41 ± 8 nm. We see that this IMFP is in excellent agreement with our calculated IMFP and that the relative difference between them is only 8 %. We note that the total IMFP for inelastic scattering in PS at 20 keV should be smaller than the experimental value due to the contributions of the 7 eV loss (about 3 %)[54] and of energy losses greater than about 40 eV (estimated to be about 10 %).

Chou and Libera measured IMFPs for polystyrene at energies of 120 keV and 200 keV using off-axis electron holography in a field-emission TEM in 2003.[55] The holographic images could be analyzed to yield energy-filtered wave-amplitude information from which Chou and Libera obtained two-dimensional images of the ratio of sample thickness to the IMFP. They used spherical polystyrene nanoparticles as samples and could calculate the sample thickness, *t*, at any point in a two-dimensional

image knowing the center and radius of the projected nanosphere. The thickness contribution to t/λ was removed to obtain quantitative IMFP values. Figure 11(B) shows their IMFPs for PS as solid circles together with our IMFPs. The Chou and Libera IMFPs are smaller than our IMFPs by 44 % and 48 % at 120 keV and 200 keV, respectively. The authors comment that their IMFP values could be systematically smaller than expected from an empirical formula because these IMFPs include the contributions of phonon excitations and because there could be some reduction in the intensity of elastically scattered electrons in their experiments.[55]

Before discussing the comparisons in Figs. 11(C) and 11(D), we need to point out that the IMFP results shown in these Figures were obtained from experiments with relatively low electron energies where the experimental energy scales were referenced to the vacuum level. For comparisons with our calculated IMFPs where the energy scale is referenced to the bottom of the conduction band, we make use of the escape barrier of 1.0 eV estimated by Signorell.[56] We have therefore increased the electron energies shown in Refs. 57 and 58 by 1 eV.

Figure 11(C) shows a comparison of our IMFPs for 26-n-paraffin to the IMFPs for squalene, $C_{30}H_{50}$ that were measured by Kostko *et al*.[57] using XPS with velocity map imaging. We make this comparison since squalene is chemically similar to 26-n-paraffin ($C_{26}H_{54}$). Kostko *et al*. measured C 1s photoelectron spectra and secondary-electron spectra from unsupported squalene nanoparticles excited by X-rays with energies between 280 eV and 345 eV. They determined relative IMFPs for energies between 13 eV and 53 eV from ratios of the C 1s intensity to the secondary-electron intensity. These relative IMFPs were converted to absolute IMFPs by normalization to our previously calculated IMFP for 26-n-paraffin of 0.7 nm at 50 eV.[4] Our calculated IMFPs for 26-n-

paraffin agree well with the squalene IMFPs for energies between 33 eV and 53 eV, and the relative difference between them is less than 6 %. For energies less than 28 eV, the IMFPs of Kostko *et al.* are smaller than our IMFPs. This difference must be due to the contributions of phonon excitations to the measured IMFPs. Our calculated IMFPs with the FPA-BABC algorithm include only electronic excitations, as indicated by Eqn. (6).

Schild *et al.*[58] reported IMFPs for water and electron energies between 11 eV and 301 eV. These IMFPs were obtained from *ab initio* calculations of electron scattering in water clusters of varying size, photoelectron angular distribution (PAD) data measured by Thürmer *et al.,*[59] EAL data measured by Suzuki *et al.*,[60] and Monte Carlo (MC) electron-trajectory calculations. Both sets of measured data were obtained from XPS measurements of the O 1s orbital of liquid water in microjets. In their approach, the IMFP and the elastic mean free path are parameters to be determined from comparisons of the two sets of experimental data and the corresponding results from MC calculations. The resulting IMFPs for water are shown in Fig 11(D) as solid red circles. These IMFPs are larger than our calculated IMFPs by factors between 2.4 and 2.8 for energies between about 31 eV and 301 eV. The energy dependence of their IMFPs is, however, similar to that of our IMFPs in this energy range. The large difference between our IMFPs and those of Schild *et al*. must be due mainly to their use of the EAL data of Suzuki *et al*.[60] We have previously shown that these EALs are larger than expected from a predictive EAL formula by factors between 2.0 and 2.4 for energies between 50 eV and 600 eV.[7] A more detailed analysis by Jablonski and Powell[47] also indicated that the EALs of Suzuki *et al*. were much larger than expected. In addition, they pointed out that the EALs of Suzuki *et al*. are actually EALs for quantitative analysis rather than EALs for measurement of thin-film thicknesses on planar substrates, and that systematic differences between the two

types of EALs are to be expected. On the other hands, we see that the Schild *et al.* IMFP at 11 eV is smaller than our calculated IMFP at the same energy. This result must be due to the effects of phonon excitations, as discussed for 26-n-paraffin.

Signorell reported elastic and inelastic electron-scattering cross sections for liquid water between 1 eV and 1098 eV from photoelectron spectroscopy of liquid water microjets and water droplets and from detailed simulations of electron scattering using ice cross sections.[56] She compared the experimentally determined effective attenuation lengths (EALs) of Suzuki *et al*.,[60] values of the photoionization anisotropy parameter β obtained by Thürmer *et al*.,[59] Nishitani *et al*.,[61] and Hartweg *et al*.,[62] and the photoelectron velocity map images (VMIs) of Signorell *et al.*[63] with the corresponding predictions from a detailed electron-scattering model based upon a Monte Carlo solution of the transport equation using scattering cross sections (CSs) for amorphous ice for energies between 1 eV and 100 eV.[64,65] She extended the latter cross sections to higher energies using the energy dependence of the IMFPs for water published by Shinotsuka *et al*.[7] Signorell concluded that the ice cross sections of Michaud *et al*.[64, 65] with her extensions to higher energies provided the most reliable cross sections for liquid water, with maximum uncertainties on the order of a factor of two. She reported IMFPs for electronic excitations in water as well as total IMFPs that also included excitations for phonon and vibrational excitations for electron energies between 1 eV and 1098 eV.

The Signorell IMFPs are shown in Fig.11 (D) as solid squares (total IMFPs) and triangles (electronic IMFPs). This figure shows that for energies between 20 eV and 1000 eV, the energy dependence of the Signorell electronic IMFPs is in reasonable agreement with that of our IMFPs. However, her IMFPs are much larger than ours, by a factor of between three and four. In the energy range of 7 eV to 100 eV, she used the CS data of

Michaud *et al.*[64] for amorphous ice. However, the IMFPs of Michaud *et al.* for water for energies between 25 eV and 100 eV are larger than IMFPs calculated from the FPA by a factor between two and three, as reported in Fig. 10 of our previous paper.[7] The CS data used by Signorell are probably the main reason for the difference in Fig. 11(D) between our IMFPs and her inelastic IMFPs for energies between 20 eV and 100 eV. For higher energies, Signorell extrapolated the CS results of Michaud *et al.* using the energy dependence of our IMFPs from the FPA.[7] It is therefore expected that there would be a constant factor of three between her electronic IMFPs and our IMFPs. For energies below 50 eV, Signorell's total IMFPs show a different energy dependence to our IMFPs because she includes the contributions of phonon and vibrational excitations.

Finally, we would like to mention results of a novel analysis of an XPS experiment by Olivieri *et al.*[66] to evaluate the IMFP for water from the TPP-2M equation [Eqns. (11) to (13) and (15)] at an energy of 86.5 eV with respect to the vacuum level (or 87.5 eV with respect to the bottom of the conduction band). They determined the spatial distributions of Na^+ ions and halide ions with respect to depth near the air-water interface (AWI) of dilute (< 1 mol/l) aqueous solutions of NaCl, NaBr, and NaI from molecular dynamics (MD) simulations with a non-polarizable force field. These distributions showed different density distributions of the Na^+ and halide ions over a depth of 1.5 nm from the solution surface. Olivieri *et al.* performed XPS experiments with a liquid-jet source at an X-ray energy of 122 eV. At this energy, the information depth for the Na 2p photoelectrons (for 95 % of the total signal) was about 1.6 nm. The XPS measurements were thus sensitive to the calculated Na^+ and halide density profiles with respect to depth near the AWI.

The measured relative intensities of the Na 2p photoelectrons from the three halide solutions closely matched those from simulations with the NIST Database for the

Simulation of Electron Spectra (SESSA)[67,68] within the experimental uncertainties. These simulations were performed with IMFPs for each solution from the TPP-2M equation. We note that the solutions were dilute so that their IMFPs were essentially the same as for water. Olivieri *et al.* found that these IMFPs would have to be increased by 150 % to be outside their experimental uncertainties. They also concluded that acceptable IMFPs at an energy of about 80 eV would have to be between 0.7 nm and 1.6 nm. This result suggests that the electronic IMFPs of Signorell and the IMFPs of Schild *et al*. at about 80 eV in Fig. 11(D) are too large. While the experimental IMFPs of Thürmer *et al*.[59] are within the IMFP limits of Olivieri *et al*., those of Michaud *et al*.[64] are not. Olivieri *et al.* also concluded that the effective attenuation lengths reported by Suzuki *et al*.[60] were likely too high, a conclusion also reached recently by Jablonski and Powell[47]. It is important to note, however, that the conclusions of Olivieri *et al*. depend on the reliability of their MD simulations and on the reliability of their SESSA simulations.

It is, of course, difficult to make IMFP and other electron-spectroscopic measurements with liquid water, and it is not surprising that substantial differences exist among the experimental values shown in Fig. 11(D) and those we discussed previously.[7] There are also large differences among the calculated IMFPs shown in Fig. 10(H) and earlier results.[7,69] While there could be systematic uncertainties in our calculated IMFPs for water, particularly for energies less than 100 eV, we point out that IMFPs from the same FPA-BABC algorithm have been calculated for Al_2O_3, AlAs, *h*-BN, GaAs, InP, MgO, and SiO_2 and generally good agreement has been found with the corresponding measured IMFPs for energies between 100 eV and 200 keV.[8]

Reliable IMFPs for liquid water are required for important applications in radiation biology,[69,70] and atmospheric chemistry[71] We hope that it will soon be possible to obtain consistency between calculated IMFPs and IMFPs obtained from experiments.

6. Summary

We report new calculations of IMFPs with the relativistic full Penn algorithm together with the correction of the bandgap-energy effect for insulators by using the Boutboul *et al.* approach[11] (relativistic FPA-BABC approach) for 14 organic compounds (26-n-paraffin, adenine, β-carotene, diphenyl-hexatriene, guanine, Kapton, polyacetylene, poly(butene-1-sulfone), polyethylene, polymethylmethacrylate, polystyrene, poly(2-vinylpridine), thymine, and uracil) and liquid water for electron energies from 50 eV to 200 keV. These calculations were made with ELFs obtained from measured optical constants and from calculated atomic scattering factors for X-ray energies.[24]

We made a comparison of the new IMFPs with our previous IMFPs for 12 organic compounds.[4] The ratios of the new IMFPs to the earlier IMFPs for 12 compounds in Fig. 5 are within ± 6 % of unity for energies between 50 eV and 2000 eV except for polyethylene between 50 eV and 90 eV. On the other hand, we see large increases of the ratios for energies less than 30 eV for polyethylene, 26-n-paraffin, PBS, and PMMA that are due to the bandgap correction from use of the FPA-BABC algorithm, as shown by Eqns (6) to (8).

Our calculated IMFPs could be fitted to a modified form of the relativistic Bethe equation for inelastic scattering of electrons in matter for energies between 50 eV and 200 keV. The values of the RMS differences between the fitted IMFPs and the calculated IMFPs range from 0.12 % to 0.27 %, while the average value of the RMS differences for the 15

compounds was 0.17 %. This average RMS difference is smaller than the average RMS differences found in similar fits for our group of 41 elemental solids[6] (0.68 %) and 42 inorganic compounds[8] (0.60 %). Equations (11) to (13) are thus convenient analytical representations of the calculated IMFPs (e.g., for interpolation).

The calculated IMFPs were also compared with IMFPs from the relativistic version of our predictive Tanuma-Powell-Penn (TPP-2M) equation.[6] The average RMS deviation between the predicted IMFPs and the calculated IMFPs for the 15 compounds over the 50 eV to 200 keV energy range was 7.2 %. This average RMS deviation is less than that found in similar comparisons for our group of 41 elemental solids (11.9 %)[6] and for our group of 42 inorganic compounds (10.7%)[8] for the same energy range. We conclude that the relativistic TPP-2M formula is useful for estimating IMFPs in solid materials for energies between 50 eV and 200 keV although the accuracy of these estimates is likely to be poorer for energies less than about 200 eV.

We compared our IMFPs for guanine and water at electron energies between 5 eV (for guanine) or 10 eV (for water) and 2000 eV to the IMFPs that were calculated with the Mermin-Penn algorithm.[29] This algorithm includes the plasmon damping factor and is useful for determining the effect of plasmon damping on IMFP calculations with the FPA-BABC approach. We conclude that the effect of plasmon damping on IMFPs calculations with the FPA-BABC approach are generally small (< 3%) for energies over 50 eV even for a material with a damping coefficient as large as that estimated for Au (2.0 eV).[29].

We also made a comparison of our IMFPs for 15 compounds with results from other calculations for energies typically between 10 eV and 10 keV. There was generally satisfactory agreement for energies between 200 eV and 10 keV. For energies less than 200 eV, our IMFPs were generally smaller than other calculated values. This difference could

be attributed to the presence or absence of an exchange correction, to single-electron excitations, to the use of different ELFs, or to other features of the chosen algorithms.

We compared our IMFPs for polyacetylene (PA), polystyrene, and 26-n-paraffin with the corresponding measured IMFPs that were determined from elastic-peak electron spectroscopy, transmission electron energy-loss experiments, TEM measurements, and velocity map imaging soft X-ray photoelectron spectroscopy. We found reasonable agreement between our IMFPs for PA and the IMFPs of Lesiak *et al.*[50] and Gergely *et al.*[51] for energies between 200 eV and 1600 eV. However, the energy dependence of their IMFPs was different from ours. For energies over 2000 eV, the IMFPs of Lesiak *et al* were clearly larger than our IMFPs. These differences could be due to density and composition differences with depth and/or to chemical changes induced by electron bombardment during the measurements. We found excellent agreement between our IMFPs for polystyrene and the measured IMFPs at 20 keV of Swanson and Powell[54] for which the relative difference was only 8 %. The IMFPs of Chou and Libera[55] for PS, however, were smaller than our IMFPs by 44 % and 48 % at 120 keV and 200 keV, respectively.

We compared our IMFPs for water with the experimental IMFPs that were determined from the photoelectron angular distribution (PAD) and EAL data together with Monte Carlo electron-trajectory calculations and from experimental information available from photoelectron spectroscopy of liquid water microjets and water droplets with detailed electron-scattering simulations using ice cross sections. We found that the experimental IMFPs of Schild *et al*.[58] and the electronic IMFPs of Signorell[56] for water were larger than our IMFPs by factors between two and four for energies between about 30 eV and 1000 eV. The energy dependences of their IMFPs, however, were similar to the energy dependence

of our IMFPs in this energy range. The large differences between their IMFPs and our values are mainly due to use of the EAL data of Suzuki *et al*.[60] by Schild *et al*. and to use of the ice IMFP data of Michaud *et al*.[64] by Signorell. We have shown that the EALs of Suzuki *et al.* and the IMFPs of Michaud *et al*. are systematically larger than our previously calculated EALs and IMFPs for water by factors of over two.[7] In addition, Jablonski and Powell[47] have recently pointed out that the EAL values of Suzuki *et al*. are actually EALs for quantitative analysis rather than EALs for measurement of thin-film thicknesses on planar substrates, and that systematic differences between the two types of EALs are to be expected. The EALs of Suzuki *et al*. were also found to be systematically too high in an analysis by Olivieri *et al.*[66] who compared measured relative intensities of Na 2p photoelectrons from three dilute halide solutions at about 80 eV with values expected from SESSA simulations based on Na^+ distributions with depth expected from molecular dynamics calculations. In addition, Olivieri *et al*. concluded that IMFPs for water from the TPP-2M equation at an energy of 82 eV were consistent with their results.

Acknowledgments

We thank Prof. Kazuo Endo for the calculations of valence-band energies for eleven of our organic compounds with Gaussian 09. We also thank Profs. D. Emfietzoglou, H. T. Nguyen-Truong, R. Signorell, and H. J. Wörner for sending their numerical IMFP data for water. We also thank Prof. R. Garcia-Molina for providing useful information on their IMFP calculations, Prof. Signorell for helpful information on her analysis of electron transport in water, and Dr. J. Villarrubia for helpful comments.

ORCID

Hiroshi Shinotsuka https://orcid.org/0000-0001-5147-1396

Shigeo Tanuma https://orcid.org/0000-0003-2628-9941

C. J. Powell https://orcid.org/0000-0001-8990-2286

Table 1. Values of the material parameters used in the IMFP calculations and in the analysis of IMFP results for the 14 organic compounds and liquid water.

Compound	Chemical formula for compound or monomer	M	ρ (g cm^{-3})	N_v	E_p (eV)	E_g (eV)	E_v (eV)	Z
26-n-paraffin	$C_{26}H_{54}$	366.6920	0.99 [4]	158	18.82	6.0	14.5	210
Adenine	$C_5H_5N_5$	135.14	1.345 [77]	50	20.33	3.8	14.8	70
β-Carotene	$C_{40}H_{56}$	536.85	0.993 [4]	216	18.21	0.0	18.7	296
Diphenyl-hexatriene	$C_{18}H_{16}$	232.3	0.986 [4]	88	17.61	0.0	18.3	124
Guanine	$C_5H_5N_5O$	151.13	1.58 [78]	56	22.05	2.5	14.5	78
Kapton	$C_{22}H_{10}N_2O_5$	382.32	1.42 [72]	138	20.63	2.04	18.8	196
Polyacetylene	C_2H_2	26.036	1.13 [a]	10	18.98	1.4	17.7	14
Poly(butene-1-sulfone)	$C_4H_8SO_2$	120.17	1.39 [81]	42	20.08	6.0	18.0	64
polyethylene	C_2H_4	28.0538	0.92 [73]	12	18.08	7.35	15.5	16
Polymethylmethacrylate	$C_5H_8O_2$	100.114	1.188 [74]	40	19.85	5.0	15.8	54
Polystyrene	C_8H_8	104.1440	1.05 [83]	40	18.30	4.5	17.0	56
Poly(2-vinylpridine)	C_7H_7N	105.136	1.14 [b]	40	18.98	4.0	16.1	40
Thymine	$C_5N_2H_6O_2$	125.11	1.36 [85]	48	20.82	3.6	12.9	66
Uracil	$C_4N_2H_4O_2$	112.092	1.40 [85]	42	20.87	3.4	14.9	58
Water	H_2O	18.0152	0.999973 [7]	8	19.20	7.9	10.0	10

a: calculated from unit cell constants taken from Ref. 75

b: Estimated by assuming that the f-sum rule [Eq. (9)] was satisfied.

Table 2. Sources of optical data used in the IMFP calculations for the 14 organic compounds and for liquid water.

Compound	Photon energy range (eV)	Source of data
26-n-paraffin	6.12 eV to 32.54 eV	Okabe *et al.* [76]
	33.39 eV to 1.12 MeV	Cullen *et al*.[24]
Adenine	4.48 eV to 55.08 eV	Arakawa *et al.*[77]
	59.05 eV to 1.12 MeV	Cullen *et al*.[24]
b-carotene	0.77 eV to 37.51 eV	Okabe *et al.*[76]
	38.28 eV to 1.12 MeV	Cullen *et al*.[24]
Diphenyl-hexatriene	0.77 eV to 38.28 eV	Okabe *et al*.[76]
	39.92 eV to 1.12 MeV	Cullen *et al.*[24]
Guanine	2.89 eV to 49.16 eV	Emerson *et al*.[78]
	49.16 eV to 1.12 MeV	Cullen *et al*.[24]
Kapton	2.26 eV to 64.86 eV	Arakawa *et al*.[79]
	67.88 eV to 1.121MeV	Cullen *et al*.[24]
Polyacetylene	1.21 eV to 58.87 eV	Ritsko *et al.* [80]
	59.05 eV to 1.12 MeV	Cullen *et al.*[24]
Poly(butene-1-sulfone)	5.6 eV to 39.0 eV	Williams[81]
	39.92 eV to 1.12 MeV	Cullen *et al.*[24]
polyethylene	5.0 eV to 60.0 eV	Palik[82]
	61.75 eV to 1.12 eV	Cullen *et al*.[24]
Polymethylmethacrylate	3.42 eV to 69.69 eV	Ritsko *et al*.[74]
	75.98 eV to 1.12 MeV	Cullen *et al*.[24]
Polystyrene	4.42 eV to 60.63 eV	Inagaki *et al.* [83]
	61.75 eV to 1.12 eV	Cullen *et al*.[24]
Poly(2-vinylpridine)	4.10 eV to 32.83 eV	Ritsko *et al.*[84]
	36.13 eV to 1.12 MeV	Cullen *et al*.[24]
Thymine	3.53 eV to 32.67 eV	Isaacson *et al.* [85]
	33.39 eV to 1.12 MeV	Cullen *et al*.[24]
Uracil	2.85 eV to 33.34 eV	Isaacson *et al*. [85]
	36.13 eV to 1.12 MeV	Cullen *et al.*[24]
Water	6.0 eV to 87.0 eV	Hayashi *et al*.[42]
	88.79 eV to 1.12 MeV	Cullen *et al.*[24]

Table 3. Values of the number of electrons per molecules, Z, Z_{eff} from Eqn (9), errors in the f-sum rule, values of P_{eff} from Eqn (10), and errors in the KK-sum rule for the 14 organic compounds and liquid water. The values of Z_{eff} and P_{eff} were determined with ΔE_{max} = 1 MeV.

Compound	Z	Z_{eff}	Error in f-sum rule (%)	P_{eff}	Error in KK-sum rule (%)
26-n-paraffin	210	196.78	-6.3	1.035	3.5
Adenine	70	70.92	1.3	1.049	4.9
β-Carotene	296	297.54	0.5	1.034	3.4
Diphenyl-hexatriene	124	130.50	5.2	1.037	3.7
Guanine	78	80.34	3.0	1.056	5.6
Kapton	196	211.79	8.1	0.989	-1.1
Polyacetylene	14	15.26	9.0	0.983	-1.7
Poly(butene-1-sulfone)	64	64.24	0.4	1.012	1.2
polyethylene	16	16.37	2.3	1.000	0.0
Polymethylmethacrylate	54	51.71	-4.2	0.974	-2.6
Polystyrene	56	56.73	1.3	1.003	0.3
Poly(2-vinylpridine)	56	56.04	0.1	1.006	0.6
Thymine	66	67.57	2.4	1.011	1.1
Uracil	58	60.38	4.1	1.041	4.1
Water	10	10.60	6.0	1.037	3.7

Table 4. Calculated IMFPs for the 14 organic compounds and for liquid water as a function of electron energy *E* with respect to the bottom of the conduction band.

Inelastic mean free path (nm)

E (eV)	26-n-paraffin	Adenine	β-Carotene	Diphenyl-hexatriene	Guanine	Kapton	Polyacetylene	Poly(butene-1-sulfone)
54.6	0.699	0.639	0.645	0.645	0.619	0.703	0.539	0.716
60.3	0.690	0.628	0.641	0.641	0.605	0.687	0.536	0.703
66.7	0.689	0.625	0.643	0.643	0.597	0.678	0.538	0.698
73.7	0.696	0.629	0.651	0.651	0.597	0.676	0.543	0.701
81.5	0.708	0.638	0.664	0.664	0.601	0.680	0.553	0.710
90.0	0.726	0.652	0.683	0.682	0.611	0.688	0.566	0.724
99.5	0.749	0.671	0.706	0.706	0.625	0.702	0.583	0.743
109.9	0.776	0.694	0.733	0.733	0.644	0.721	0.602	0.767
121.5	0.809	0.721	0.765	0.765	0.667	0.745	0.626	0.795
134.3	0.847	0.753	0.801	0.801	0.694	0.773	0.653	0.829
148.4	0.889	0.789	0.842	0.842	0.725	0.806	0.685	0.867
164.0	0.937	0.829	0.887	0.888	0.760	0.844	0.721	0.910
181.3	0.991	0.875	0.938	0.939	0.800	0.887	0.761	0.958
200.3	1.05	0.925	0.994	0.995	0.845	0.935	0.806	1.01
221.4	1.12	0.981	1.06	1.06	0.894	0.988	0.856	1.07
244.7	1.19	1.04	1.12	1.13	0.949	1.05	0.910	1.14
270.4	1.27	1.11	1.20	1.20	1.01	1.11	0.971	1.21
298.9	1.35	1.18	1.28	1.28	1.08	1.18	1.04	1.29
330.3	1.45	1.27	1.37	1.37	1.15	1.26	1.11	1.38
365.0	1.55	1.36	1.47	1.47	1.23	1.35	1.19	1.47
403.4	1.66	1.45	1.58	1.58	1.32	1.45	1.27	1.57
445.9	1.79	1.56	1.69	1.70	1.41	1.55	1.37	1.69
492.7	1.92	1.68	1.82	1.82	1.52	1.66	1.47	1.81
544.6	2.07	1.80	1.96	1.96	1.63	1.79	1.58	1.95
601.8	2.23	1.94	2.11	2.11	1.75	1.92	1.71	2.09
665.1	2.40	2.09	2.28	2.28	1.89	2.07	1.84	2.25
735.1	2.60	2.26	2.46	2.46	2.04	2.23	1.98	2.43
812.4	2.80	2.43	2.65	2.66	2.20	2.40	2.14	2.62
897.8	3.03	2.63	2.87	2.87	2.37	2.59	2.32	2.83
992.3	3.27	2.84	3.10	3.10	2.56	2.80	2.50	3.05
1096.6	3.54	3.07	3.35	3.36	2.77	3.02	2.71	3.30

1212.0	3.83	3.32	3.63	3.63	3.00	3.27	2.93	3.56
1339.4	4.15	3.60	3.93	3.93	3.24	3.53	3.17	3.85
1480.3	4.49	3.90	4.25	4.26	3.51	3.82	3.44	4.17
1636.0	4.87	4.22	4.61	4.62	3.80	4.14	3.73	4.52
1808.0	5.28	4.58	5.00	5.01	4.12	4.49	4.04	4.89
1998.2	5.72	4.96	5.42	5.43	4.47	4.86	4.38	5.30
2208.3	6.21	5.38	5.88	5.89	4.84	5.27	4.75	5.75
2440.6	6.74	5.84	6.39	6.40	5.25	5.72	5.16	6.23
2697.3	7.32	6.34	6.93	6.94	5.70	6.20	5.60	6.76
2981.0	7.95	6.88	7.53	7.54	6.19	6.73	6.09	7.34
3294.5	8.63	7.47	8.18	8.19	6.72	7.31	6.61	7.97
3641.0	9.38	8.12	8.89	8.91	7.30	7.94	7.19	8.65
4023.9	10.2	8.82	9.67	9.68	7.93	8.62	7.81	9.40
4447.1	11.1	9.58	10.5	10.5	8.62	9.36	8.49	10.2
4914.8	12.0	10.4	11.4	11.4	9.36	10.2	9.23	11.1
5431.7	13.1	11.3	12.4	12.4	10.2	11.1	10.0	12.1
6002.9	14.2	12.3	13.5	13.5	11.1	12.0	10.9	13.1
6634.2	15.5	13.4	14.7	14.7	12.0	13.1	11.9	14.2
7332.0	16.9	14.6	16.0	16.0	13.1	14.2	12.9	15.5
8103.1	18.3	15.8	17.4	17.4	14.2	15.4	14.1	16.8
8955.3	19.9	17.2	18.9	18.9	15.5	16.8	15.3	18.3
9897.1	21.7	18.7	20.6	20.6	16.8	18.3	16.6	19.9
10938.0	23.6	20.4	22.4	22.4	18.3	19.9	18.1	21.7
12088.4	25.6	22.1	24.3	24.4	19.9	21.6	19.7	23.5
13359.7	27.9	24.1	26.5	26.5	21.6	23.5	21.4	25.6
14764.8	30.3	26.2	28.8	28.8	23.5	25.5	23.3	27.8
16317.6	33.0	28.5	31.3	31.3	25.5	27.7	25.3	30.2
18033.7	35.8	30.9	34.0	34.1	27.8	30.1	27.5	32.8
19930.4	38.9	33.6	37.0	37.0	30.1	32.7	29.9	35.7
22026.5	42.3	36.5	40.2	40.2	32.7	35.5	32.4	38.7
24343.0	45.9	39.6	43.6	43.7	35.5	38.6	35.2	42.0
26903.2	49.8	43.0	47.3	47.4	38.6	41.8	38.2	45.6
29732.6	54.0	46.6	51.3	51.4	41.8	45.4	41.5	49.5
32859.6	58.6	50.5	55.7	55.7	45.3	49.2	45.0	53.6
36315.5	63.5	54.7	60.3	60.4	49.1	53.3	48.7	58.1
40134.8	68.7	59.3	65.3	65.4	53.1	57.7	52.7	62.9

44355.9	74.3	64.1	70.7	70.7	57.5	62.4	57.1	68.0
49020.8	80.3	69.3	76.4	76.5	62.1	67.4	61.7	73.5
54176.4	86.8	74.8	82.5	82.6	67.1	72.8	66.6	79.4
59874.1	93.6	80.7	89.0	89.1	72.4	78.5	71.9	85.6
66171.2	101	87.0	95.9	96.0	78.0	84.6	77.5	92.2
73130.4	109	93.6	103.2	103	83.9	91.0	83.4	99.3
80821.6	117	101	111	111	90.2	97.8	89.6	107
89321.7	125	108	119	119	96.8	105	96.2	114
98715.8	134	116	128	128	104	112	103	123
109097.8	144	124	137	137	111	120	110	131
120571.7	153	132	146	146	119	129	118	140
133252.4	164	141	156	156	126	137	126	149
147266.6	174	150	166	166	134	146	134	159
162754.8	185	159	176	176	143	155	142	169
179871.9	196	169	186	186	151	164	150	179
198789.2	207	178	197	197	160	173	159	189

Table 4. continued

	Inelastic mean free path (nm)						
E (eV)	polyethylene	Polymethyl-methacrylate	Polystyrene	Poly(2-vinylpridine)	Thymine	Uracil	Water
54.6	0.723	0.783	0.697	0.695	0.635	0.598	1.035
60.3	0.710	0.767	0.689	0.684	0.624	0.592	1.007
66.7	0.707	0.761	0.688	0.681	0.619	0.591	0.989
73.7	0.711	0.763	0.694	0.685	0.622	0.596	0.981
81.5	0.721	0.772	0.706	0.696	0.630	0.605	0.981
90.0	0.737	0.788	0.723	0.712	0.642	0.618	0.988
99.5	0.758	0.809	0.745	0.733	0.659	0.636	1.00
109.9	0.785	0.835	0.771	0.758	0.681	0.657	1.02
121.5	0.816	0.867	0.803	0.789	0.707	0.682	1.05
134.3	0.853	0.903	0.839	0.824	0.737	0.712	1.09
148.4	0.894	0.945	0.881	0.864	0.771	0.745	1.13
164.0	0.941	0.993	0.927	0.910	0.810	0.783	1.18
181.3	0.994	1.05	0.979	0.960	0.854	0.825	1.23
200.3	1.05	1.10	1.04	1.02	0.903	0.872	1.30
221.4	1.12	1.17	1.10	1.08	0.957	0.925	1.37
244.7	1.19	1.24	1.17	1.15	1.02	0.982	1.44
270.4	1.27	1.32	1.25	1.22	1.08	1.05	1.53
298.9	1.35	1.41	1.33	1.30	1.16	1.12	1.63
330.3	1.45	1.50	1.42	1.39	1.23	1.19	1.74
365.0	1.55	1.61	1.53	1.49	1.32	1.28	1.86
403.4	1.66	1.72	1.64	1.60	1.42	1.37	1.99
445.9	1.78	1.85	1.76	1.72	1.52	1.47	2.13
492.7	1.92	1.99	1.89	1.85	1.63	1.58	2.28
544.6	2.06	2.14	2.03	1.99	1.76	1.70	2.45
601.8	2.22	2.30	2.19	2.14	1.89	1.83	2.64
665.1	2.39	2.48	2.36	2.31	2.04	1.97	2.84
735.1	2.58	2.67	2.54	2.49	2.20	2.12	3.06
812.4	2.79	2.88	2.75	2.69	2.37	2.29	3.30
897.8	3.01	3.11	2.97	2.90	2.57	2.47	3.56
992.3	3.26	3.36	3.21	3.14	2.77	2.67	3.85
1096.6	3.52	3.63	3.47	3.39	3.00	2.89	4.16
1212.0	3.81	3.93	3.75	3.67	3.24	3.13	4.49

1339.4	4.12	4.25	4.06	3.97	3.51	3.38	4.86
1480.3	4.47	4.60	4.40	4.30	3.80	3.67	5.26
1636.0	4.84	4.98	4.76	4.66	4.12	3.97	5.70
1808.0	5.25	5.40	5.16	5.05	4.46	4.30	6.18
1998.2	5.69	5.85	5.60	5.47	4.84	4.67	6.70
2208.3	6.17	6.35	6.07	5.94	5.25	5.06	7.26
2440.6	6.70	6.88	6.59	6.44	5.70	5.49	7.88
2697.3	7.27	7.47	7.15	6.99	6.18	5.96	8.55
2981.0	7.89	8.11	7.77	7.59	6.71	6.47	9.28
3294.5	8.57	8.81	8.44	8.24	7.29	7.03	10.1
3641.0	9.32	9.57	9.17	8.96	7.92	7.64	10.9
4023.9	10.1	10.4	9.96	9.73	8.61	8.30	11.9
4447.1	11.0	11.3	10.8	10.6	9.35	9.02	12.9
4914.8	12.0	12.3	11.8	11.5	10.2	9.80	14.0
5431.7	13.0	13.3	12.8	12.5	11.1	10.7	15.2
6002.9	14.1	14.5	13.9	13.6	12.0	11.6	16.6
6634.2	15.4	15.8	15.1	14.8	13.1	12.6	18.0
7332.0	16.7	17.1	16.5	16.1	14.2	13.7	19.6
8103.1	18.2	18.6	17.9	17.5	15.5	14.9	21.3
8955.3	19.8	20.3	19.5	19.0	16.8	16.2	23.1
9897.1	21.5	22.0	21.2	20.7	18.3	17.6	25.1
10938.0	23.4	24.0	23.0	22.5	19.9	19.2	27.3
12088.4	25.4	26.1	25.0	24.5	21.6	20.8	29.7
13359.7	27.7	28.3	27.2	26.6	23.5	22.7	32.3
14764.8	30.1	30.8	29.6	28.9	25.5	24.6	35.1
16317.6	32.7	33.5	32.2	31.4	27.8	26.8	38.1
18033.7	35.5	36.4	35.0	34.2	30.2	29.1	41.4
19930.4	38.6	39.5	38.0	37.1	32.8	31.6	45.0
22026.5	41.9	42.9	41.3	40.3	35.6	34.3	48.9
24343.0	45.5	46.6	44.8	43.7	38.6	37.3	53.0
26903.2	49.4	50.5	48.6	47.5	41.9	40.4	57.5
29732.6	53.6	54.8	52.7	51.5	45.5	43.9	62.4
32859.6	58.1	59.4	57.2	55.8	49.3	47.6	67.6
36315.5	62.9	64.4	61.9	60.5	53.4	51.5	73.2
40134.8	68.1	69.7	67.1	65.5	57.8	55.8	79.3
44355.9	73.7	75.4	72.5	70.8	62.5	60.3	85.7

49020.8	79.6	81.5	78.4	76.6	67.6	65.2	92.7
54176.4	86.0	88.0	84.7	82.7	73.0	70.4	100
59874.1	92.8	94.9	91.4	89.2	78.7	76.0	108
66171.2	100	102	98.4	96.1	84.8	81.9	116
73130.4	108	110	106	103	91.3	88.1	125
80821.6	116	118	114	111	98.1	94.7	134
89321.7	124	127	122	119	105	102	144
98715.8	133	136	131	128	113	109	155
109097.8	142	146	140	137	121	117	165
120571.7	152	155	150	146	129	124	177
133252.4	162	166	160	156	137	133	188
147266.6	172	176	170	166	146	141	200
162754.8	183	187	180	176	155	150	212
179871.9	194	198	191	186	165	159	225
198789.2	205	209	202	197	174	168	238

Table 5. Values of the parameters β, γ, C, D found in the fits of Equation (11) to the calculated IMFPs for each organic compound and liquid water for electron energies between 50 eV and 200 keV and values of *RMS* calculated from Eqn (14).

Compound	β (eV^{-1} nm^{-1})	γ (eV^{-1})	C (nm^{-1})	D (eV nm^{-1})	*RMS* (%)
26-n-paraffin	0.1696	0.1664	12.15	207.3	0.15
Adenine	0.1699	0.1557	13.22	257.8	0.17
β-Carotene	0.1895	0.1749	14.41	277.5	0.22
Diphenyl-hexatriene	0.2025	0.1739	15.16	285.8	0.22
Guanine	0.1619	0.1484	13.54	271.7	0.13
Kapton	0.1716	0.1398	15.31	341.7	0.17
Polyacetylene	0.2150	0.1813	18.57	383.6	0.12
Poly(butene-1-sulfone)	0.1670	0.1338	12.79	275.4	0.27
polyethylene	0.1862	0.1609	13.92	245.1	0.15
Polymethylmethacrylate	0.1525	0.1465	12.11	245.8	0.20
Polystyrene	0.1846	0.1604	13.89	264.5	0.19
Poly(2-vinylpridine)	0.1762	0.1576	13.24	245.5	0.18
Thymine	0.1657	0.1581	13.40	260.1	0.12
Uracil	0.1707	0.1597	14.30	306.1	0.14
Water	0.1431	0.1474	15.00	356.6	0.10

Table 6. Root-mean-square (RMS) deviations between IMFPs from the relativistic TPP-2M equation [Eqn (15)] and IMFPs calculated from optical data for energies between 50 eV and 200 keV.

Compound	RMS deviation (%)
26-n-paraffin	1.9
Adenine	1.8
β-Carotene	11.4
Diphenyl-hexatriene	13.0
Guanine	9.2
Kapton	4.9
Polyacetylene	10.1
Poly(butene-1-sulfone)	2.7
polyethylene	7.1
Polymethylmethacrylate	10.1
Polystyrene	8.7
Poly(2-vinylpridine)	8.3
Thymine	4.2
Uracil	6.5
Water	8.3

Figure Captions

Figure 1. Plots of our calculated inelastic mean free paths as a function of electron kinetic energy for 26-n-paraffine, adenine, β-carotene, and diphenyl-hexatriene. The solid circles show calculated IMFPs from the relativistic full Penn algorithm using the Boutboul *et al.* approach (Table 4). The solid lines show fits to these IMFPs with the relativistic modified Bethe equation [Eqns. (11) to (13)] and the derived parameters are listed in Table 5. The long-dashed lines indicate IMFPs calculated from the relativistic TPP-2M equation [Eqs. (11) to (13) and (15)].

Figure 2. Plots of our calculated inelastic mean free paths as a function of electron kinetic energy for guanine, Kapton, polyacetylene, and poly(butone-1-sulfone). See caption to Fig. 1.

Figure 3. Plots of our calculated inelastic mean free paths as a function of electron kinetic energy for polyethylene, PMMA, polystyrene, and poly(2-vinylpyridine). See caption to Fig. 1.

Figure 4. Plots of our calculated inelastic mean free paths as a function of electron kinetic energy for thymine, uracil and water. See caption to Figure 1.

Figure 5. Plots of ratios of IMFPs for 12 organic compounds calculated from the relativistic FPA-BABC algorithm to the previous IMFPs.[4]

Figure 6. Plots of the optical energy loss functions for polyacetylene, polyethylene, and polystyrene in the energy range between 0 eV and 100 eV.

Figure 7. Plots of calculated IMFPs from the relativistic FPA-BABC approach (solid circles) and the relativistic FPA with E_g assumed to be zero for polyacetylene (solid line), polyethylene (dashed line), and polystyrene (dotted line) as a function of electron kinetic energy between 3 eV and 100 eV.

Figure 8. Ratio of IMFPs calculated from the relativistic TPP-2M equation [Eqns. (11), (12), (13) and (15)] to IMFPs calculated from optical data with the relativistic FPA-BABC approach as a function of electron energy for our 14 inorganic compounds (solid squares) and liquid water (solid circles).

Figure 9. (A), (B) Plots of calculated electron IMFPs from the Mermin-Penn-BABC approach with damping factor γ_D = 0.2 eV, 1.0 eV, 1.5 eV, and 2.0 eV [in Eqns. (17) and (18)] and from FPA-BABC approach for guanine (A) and water (C) as a function of electron kinetic energy between 5 eV (guanine) or 10 eV (water) and 10 keV. (B), (D) Ratios of IMFPs calculated from the Mermin-Penn-BABC approach to our IMFPs as a function of electron energy for guanine (B) and water (D).

Figure 10. Comparison of our calculated IMFPs with IMFPs from other calculations for (A) 26-n-paraffin and adenine, (B) β-carotene and DHT, (C) guanine and Kapton, (D) polyacetylene and poly(butone-1-sulfone), (E) polyethene and

PMMA, (F) polystyrene and poly(2-vinylpyridine), (G) thymine and uracil, and (H) liquid water for energies between 5 eV or 10 eV (for water) and 10 keV. The solid lines show our IMFPs that were calculated from optical ELFs with the relativistic FPA-BABC algorithm. The dashed line shows the IMFPs for liquid water that were calculated from optical ELFs with the relativistic FPA. The symbols indicate IMFPs calculated by Akkerman *et al*.[30] (for 26-n-paraffin, β-carotene, diphenyl-hexatriene (DHT), guanine, polyacetylene, poly(butone-1-sulfone), polyethylene, PMMA, polystyrene, and poly(2-vinylpyridine), Tan *et al*.[33] (for adenine, guanine, thymine and uracil), Garcia-Molina *et al*.[37] (for β-carotene and liquid water), de Vera *et al*.[36] (for Kapton, polyacetylene, PMMA, and poly(2-vinylpyridine)), Emfietzoglou *et al*.[39] (for water), Nguyen-Troung[40] (for water), and Flores-Mancera *et al*.[41] (for water).

Figure 11. Comparison of our calculated IMFPs with measured IMFPs for (A) polyacetylene, (B) polystyrene, (C) 26-n-paraffin, and (D) water. The solid lines show our IMFPs that were calculated from optical ELFs with the relativistic FPA-BABC approach. The symbols indicate IMFPs measured by Gergely *et al*.[51] and Lesiak *et al*.[50] (for polyacetylene), by Chou and Libera[55] and Swanson and Powell[54] (for polystyrene), by Kostko *et al.*[57] (for squalene), and by Schild *et al.*[58] and Signorell (for water)[56].

References

[1] Tanuma S, Powell CJ, Penn DR. Calculations of electron inelastic mean free paths. *Surf Interface Anal.* 1988; 11(11): 577-589. https://doi.org/10.1002/sia.740111107.

[2] Tanuma S, Powell CJ, Penn DR. Calculations of electron inelastic mean free paths. II. Data for 27 elements over the 50 – 2000 eV range. *Surf. Interface Anal.* 1991; 17(13): 911-926. https://doi.org/10.1002/sia.740171304.

[3] Tanuma S, Powell CJ, Penn DR. Calculations of electron inelastic mean free paths. III. Data for 15 inorganic compounds over the 50–2000 eV range. *Surf. Interface Anal.* 1991; 17(13): 927-939. https://doi.org/10.1002/sia.740171305.

[4] Tanuma S, Powell CJ, Penn DR. Calculations of electron inelastic mean free paths. V. Data for 14 organic compounds over the 50–2000 eV range. *Surf. Interface Anal.* 1994; 21(3): 165-176. https://doi.org/10.1002/sia.740210302.

[5] Tanuma S, Powell CJ, Penn DR. Calculations of electron inelastic mean free paths. IX. Data for 41 elemental solids over the 50 eV to 30 keV range. *Surf. Interface Anal.* 2011; 43(3): 689-713. https://doi.org/10.1002/sia.3522.

[6] Shinotsuka H, Tanuma S, Powell CJ, Penn DR. Calculations of electron inelastic mean free paths. X. Data for 41 elemental solids over the 50 eV to 200 keV range with the relativistic full Penn algorithm. *Surf Interface Anal.* 2015; 47(9): 871-888. https://doi.org/10.1002/sia.5789; *ibid*, *Surf. Interface Anal.,* 2015, 47(12), 1132. https://doi.org/10.1002/sia.5861.

[7] Shinotsuka H, Tanuma S, Powell CJ, Penn DR. Calculations of electron inelastic mean free paths. XI. Data for liquid water for energies from 50 eV to 30 keV. *Surf Interface Anal.* 2017; 49(4): 238-252. https://doi.org/10.1002/sia.6123.

[8] Shinotsuka H, Tanuma S, Powell CJ, Penn DR. Calculations of electron inelastic mean free paths. XII. Data for 42 inorganic compounds over the 50 eV to 200 keV range with the full Penn algorithm. *Surf Interface Anal.* 2019; 51(4): 427-457. https://doi.org/10.1002/sia.6598.

[9] Penn DR. Electron mean-free-path calculations using a model dielectric function, *Phys. Rev. B.*1987; 35(2): 482-486. https://doi.org/10.1103/PhysRevB.35.482.

[10] Bethe H. Zur Theorie des Durchgangs schneller Korpuskularstrahlen durch Materie. *Ann. Phys.* 1930; 397(3): 325-400. https://doi.org/10.1002/andp.19303970303.

[11] Boutboul T, Akkerman A, Breskin A, Chechik R. Electron inelastic mean free path and stopping power modelling in alkali halides in the 50 eV–10 keV energy range. *J. Appl. Phys.* **1996**; 79: 6714. https://doi.org/10.1063/1.361491.

[12] Tahir D, Tougaard S. Electronic and optical properties of selected polymers studied by reflection electron energy loss spectroscopy. *J. Appl. Phys.* 2012; 111: 054101. http://dx.doi.org/10.1063/1.3688327

[13] Fernandez-Varea M, Liljequist D, Csillag S, Raty R, Salvat F. Monte Carlo simulation of 0.1–100 keV electron and positron transport in solids using optical data and partial wave methods. *Nucl. Instrum. Methods Phys. Res. B.* 1996; 108(1-2): 35 – 50. https://doi.org/10.1016/0168-583X(95)01055-6

[14] Fano U. Penetration of Protons, Alpha Particles, and Mesons. *Ann. Rev. Nucl. Sci*. 1963; 13; 1-66. https://doi.org/10.1146/annurev.ns.13.120163.000245

[15] Lindhard J. On the Properties of a Gas of Charged Particles. *K. Dan. Vidensk. Selsk. Mat.-Fys. Medd*. **1954** ; 28(8): 1- 57.

[16] Kumar V, Goyal PK, Gupta R, Kumar S. Tailoring of optical band gap and refractive index of heat treated Kapton-H Polyimide. *Advances in Applied Science Research*, 2011; 2 (2): 79-85. https://www.imedpub.com/articles/tailoring-of-optical-band-gap-and-refractive-index-of-heat-treated-kaptonh-polyimide.pdf.

[17] Hüfner S. *Photoelectron Spectroscopy -Principles and Applications.* third ed. New York: Springer; 2003. https://doi.org/10.1007/978-3-662-09280-4

[18] Tanaka T. Optical absorption and electrical conduction in polyethylene. J*ournal of Applied Physics.* 1973; 44: 2430. https://doi.org/10.1063/1.1662586

[19] Isaacson M. Interaction of 25 keV Electrons with the Nucleic Acid Bases, Adenine, Thymine, and Uracil. I. Outer Shell Excitation. *J. Chem. Phys..* 1972; 56: 1803-1812. https://doi.org/10.1063/1.1677456

[20] Gaussian 09, Revision E.01, Frisch, M. J.; Trucks, G. W.; Schlegel, H. B.; Scuseria, G. E.; Robb, M. A.; Cheeseman, J. R.; Scalmani, G.; Barone, V.; Mennucci, B.;

Petersson, G. A.; Nakatsuji, H.; Caricato, M.; Li, X.; Hratchian, H. P.; Izmaylov, A. F.; Bloino, J.; Zheng, G.; Sonnenberg, J. L.; Hada, M.; Ehara, M.; Toyota, K.; Fukuda, R.; Hasegawa, J.; Ishida, M.; Nakajima, T.; Honda, Y.; Kitao, O.; Nakai, H.; Vreven, T.; Montgomery, J. A., Jr.; Peralta, J. E.; Ogliaro, F.; Bearpark, M.; Heyd, J. J.; Brothers, E.; Kudin, K. N.; Staroverov, V. N.; Kobayashi, R.; Normand, J.; Raghavachari, K.; Rendell, A.; Burant, J. C.; Iyengar, S. S.; Tomasi, J.; Cossi, M.; Rega, N.; Millam, J. M.; Klene, M.; Knox, J. E.; Cross, J. B.; Bakken, V.; Adamo, C.; Jaramillo, J.; Gomperts, R.; Stratmann, R. E.; Yazyev, O.; Austin, A. J.; Cammi, R.; Pomelli, C.; Ochterski, J. W.; Martin, R. L.; Morokuma, K.; Zakrzewski, V. G.; Voth, G. A.; Salvador, P.; Dannenberg, J. J.; Dapprich, S.; Daniels, A. D.; Farkas, Ö.; Foresman, J. B.; Ortiz, J. V.; Cioslowski, J.; Fox, D. J. Gaussian, Inc., Wallingford CT, 2009.

[21] Feyer V, Plekan O, Šutara F, Cháb V, Matolín V, Prince KC. Guanine adsorption on the Cu (110) surface. *Surface Science.* 2011; 605: 361-365. https://doi.org/10.1016/j.susc.2010.11.002

[22] G. Beamson and D. Briggs .High resolution XPS of organic polymers, the scienta ESCA300 database. Wiley, Chichester 1992. https://doi.org/10.1002/adma.19930051035

[23] Stewart JJP. Optimization of parameters for semiempirical methods VI: more modifications to the NDDO approximations and re-optimization of Parameters. *J. Molec. Modeling*. 2013; 19:1-32. https://doi.org/10.1007/s00894-012-1667-x.

[24] Cullen DE, Hubbell JH, Kissel L., *EPDL97, T*he Evaluated Data Library, 1997 Version, UCRL-50400, Vol. 6, Rev. 5 (Sep 19, 1997). http://ftp.esrf.eu/pub/scisoft/xop2.3/DabaxFiles/.

[25] Tanuma S, Powell CJ, Penn DR. Electron inelastic mean free paths in solids at low energies. *J. Electron Spectrosc. Relat. Phenom.* **1990**; 52: 285-291. https://doi.org/10.1016/0368-2048(90)85024-4.

[26] Henke BL, Lee P, Tanaka TJ, Shimabukuro RL, Fujikawa BK. Low-energy x-ray interaction coefficients: Photoabsorption, scattering, and reflection: E = 100–2000 eV Z = 1–94. *Data Nucl. Data Tables* 1982; 27(1): 1-144.

https://doi.org/10.1016/0092-640X(82)90002-X

[27] Abril I, Garcia-Molina R, Denton CD, Pe´rez-Pe´rez FJ, Arista NR. Dielectric description of wakes and stopping powers in solids. *Phys. Rev. A*. 1988; 58; 357. https://doi.org/10.1103/PhysRevA.58.357

[28] Chantler CT, Bourke JD. Electron Inelastic Mean Free Path Theory and Density Functional Theory Resolving Discrepancies for Low-Energy Electrons in Copper. *J. Phys. Chem. A* 2014;118(5): 909–914. https://doi.org/10.1021/jp408438r.

[29] Nguyen-Truong HT, Penn Algorithm Including Damping for Calculating the Electron Inelastic Mean Free Path. *J. Phys. Chem. C* 2015; 119: 7883−7887. https://doi.org/10.1021/acs.jpcc.5b00403

[30] Akkerman A, Akkerman E. Characteristics of electron inelastic interactions in organic compounds and water over the energy range 20–10000 eV. *J. Appl. Phys*.1999; 86(10): 5809 – 5816. https://doi.org/10.1063/1.371597.

[31] Ashley JC. Energy-loss probabilities for electrons, positrons, and protons in condensed matter. *J. Appl. Phys*.1991; 69(2): 674 – 678. https://doi.org/10.1063/1.347348.

[32] Powell CJ, Jablonski A, Evaluation of Calculated and Measured Electron Inelastic Mean Free Paths Near Solid Surfaces. *J. Phys. Chem. Ref. Data*, 1999; 28: 19. https://doi.org/10.1063/1.556035.

[33] Tan Z, Xia Y, Liu X, Zhao M, Ji Y, Li F, Huang B. Cross sections of electron inelastic interactions in DNA. *Radiat Environ Biophys*. 2004; 43: 173–182. https://doi.org/10.1007/s00411-004-0249-4

[34] Ochkur VI. The Born-Oppenheimer method in the theory of atomic collisions. *Sov. Phys. JETP.* 1964; 18(2): 503-508.

[35] Fernandez-Varea JM, Mayol R, Liljequist D, Salvat F. Inelastic scattering of electrons in solids from a generalized oscillator strength model using optical and photoelectric data. *J. Phys.: Condens. Matter.*1993; 5(22): 3593. https://doi.org/10.1088/0953-8984/5/22/011

[36] de Vera P, Abril I, Garcia-Molina. Inelastic scattering of electron and light ion in organic polymers. *J. Appl. Phys*.2011; 109: 094901.

https://doi.org/10.1063/1.3581120

[37] Garcia-Molina R, Abril I, Kyriakou I, Emfietzoglou D. Inelastic scattering and energy loss of swift electron beams in biologically relevant materials. *Surf. Interface Anal.* 2017; 49; 11–17. https://doi.org/10.1002/sia.5947

[38] Sun SQ, SHI S-L, Hunt JA, Leapman RD. Quantitative water mapping of cryosectioned cells by electron energy-loss spectroscopy. *Journal of Microscopy.* 1995; 177(1): 18 – 30. https://doi.org/10.1111/j.1365-2818.1995.tb03530.x

[39] Emfietzoglou D, Papamichael G, Nikjoo H. Monte Carlo Electron Track Structure Calculations in Liquid Water Using a New Model Dielectric Response Function. *Radiation Research*. 2017; 188(3): 355-368. https://doi.org/10.1667/RR14705.1

[40] Nguyen-Truong HT. Low-energy electron inelastic mean free paths for liquid water. *Journal of Physics: Condensed Matter*. 2018; 30(15): 155101. https://doi.org/10.1088/1361-648x/aab40a.

[41] Miguel Angel Flores-Mancera, John S. Villarrubia, and Guerda Massillon-JL. Electron Inelastic Mean Free Paths for LiF, CaF_2, Al_2O_3, and Liquid Water from 433 keV down to the Energy Gap. *ACS Omega*. 2020; 5 (8): 4139-4147. https://doi.org/10.1021/acsomega.9b03872

[42] Hayashi H, Watanabe N, Udagawa Y, Kao C-C. The complete optical spectrum of liquid water measured by inelastic x-ray scattering. *Proc. Nat. Acad. Sciences*, 2000; 97: 6264-6266. https://doi.org/10.1073/pnas.110572097

[43] Fernandez-Varea JM, Mayol R, Liljequist D, Salvat F. Inelastic scattering of electrons in solids from a generalized oscillator strength model using optical and photoelectric data. *J. Phys.: Condens.Matter.* 1993; 5(22); 3593. https://doi.org/10.1088/0953-8984/5/22/011.

[44] Watanabe N, Hayshi H, Udagawa Y. Bethe Surface of Liquid Water determined by Inelastic X-ray Scattering Spectroscopy and Electron Correlation Effect. *Bull. Chem. Soc. Jpn.* 1997; 70: 719-726. https://doi.org/10.1246/bcsj.70.719.

[45] Ashley JC. Optical-data model for the stopping power of condensed matter for protons and antiprotons. *J. Phys.: Condens. Matter* . 1991; 3 :2741.

https://doi.org/10.1088/0953-8984/3/16/014

[46] Bethe HA, Ashkin J, *Experimental Nuclear Physics*, Vol 1, Wiley, New York. 1953, pp. 166-357; Davydov AS, Quantum Mechanics, Adison-Wesley, Reading, MA, 1968, pp. 404-406.

[47] Jablonski A, Powell CJ. Effective Attenuation Lengths for Different Quantitative Applications of X-ray Photoelectron Spectroscopy. *J. Phys. Chem. Ref. Data.* 2020; 49: 033102. https://doi.org/10.1063/5.0008576.

[48] Winter B , Weber R, Widdra W, Dittmar M, Faubel M, Hertel IV. Full Valence Band Photoemission from Liquid Water Using EUV Synchrotron Radiation. *J. Phys. Chem.* 2004; 108:2625. https://doi.org/10.1021/jp030263q

[49] Signorell R, Goldmann M, Yoder BL, Bodi A, Chasovskish E, Lang L, Luckhaus D. Nanofocusing, shadowing, and electron mean free path in the photoemission from aerosol droplets. *Chem. Phys. Lett.* 2016; 658:1. https://10.1016/j.cplett.2016.05.046

[50] Lesiak B, Kosinski A, Krawczyk M, Zommer L, Jablonski A, Kövér L, Tóth J, Varga D, Cserny I, Zemek J, Jiricek P. Characterization of Polyacetylene and Polyacetylene Doped with Palladium. *Polish J. Chem.* 2000; 74: 847–865.

[51] Gergely G, Menyhard M, Sulyok A, Gurban S, Lesiak B, Jablonski A, Kosinski A, Toth J, Varga D. Evaluation of the inelastic mean free path (IMFP) of electrons in polyaniline and polyacetylene samples obtained from elastic peak electron spectroscopy (EPES). *Central European Journal of Physics* 2007; 5: 188–200. https://doi.org/10.2478/s11534-007-0012-y

[52] Chen Y-F. (2002). Surface effects on angular distributions in X-ray-photoelectron spectroscopy. Surface Science. 2002; 519(1-2): 115-124. https://doi.org/10.1016/S0039-6028(02)02206-9

[53] Chapiro A. Chemical modifications in irradiated polymers. Nucl. Instr. Methods Phys. Res. B. 1988; 32(1-4): 111-114. https://doi.org/10.1016/0168-583X(88)90191-7

[54] Swanson N, Powell CJ. Inelastic scattering cross sections for 20 keV electrons in Al, Be, and polystyrene. *Phys. Rev.* 1966; 145:195- 208. https://doi.org/10.1103/PhysRev.145.195

[55] Chou TM, Libera M. Mean free paths for inelastic electron scattering in silicon and poly(styrene) nanospheres. *Ultramicroscopy*. 2003: 94; 31-35. https://doi.org/10.1016/S0304-3991(02)00192-4

[56] Signorell R. Electron Scattering in Liquid Water and Amorphous Ice: A Striking Resemblance. Phys. Rev. Lett. 2020; **124**: 205501. https://link.aps.org/doi/10.1103/PhysRevLett.124.205501.

[57] Kostko O, Jacobs MI, Xu B, Wilson KR, Ahmed M. Velocity map imaging of inelastic and elastic low energy electron scattering in organic nanoparticles. *J. Chem. Phys.* 2019: 151, 184702. https://doi: 10.1063/1.5126343.

[58] Schild A, Peper M, Perry C, Ratthenbacher D, Worner HJ. Alternative Approach for the Determination of Mean Free Paths of Electron Scattering in Liquid Water Based on Experimental Data. *J. Phys. Chem. Lett.* 2020; 11(3) : 1128–1134. https://doi.org/10.1021/acs.jpclett.9b02910

[59] Thürmer S, Seidel R, Faubel M, Eberhardt W, Hemminger JC, Bradforth SE, Winter B. Photoelectron Angular Distributions from Liquid Water: Effects of Electron Scattering. *Phys*. *Rev*. *Letters* 2013; 111: 173005. https://doi.org/10.1103/PhysRevLett.111.173005

[60] Suzuki Y, Nishizawa K, Kurahashi N, Suzuki T. Effective attenuation length of an electron in liquid water between 10 and 600 eV. *Phys. Rev*. *E*. 2014; *90*: 010302(R). https://doi.org/10.1103/PhysRevE.90.010302

[61] Nishitani J, West WC, Suzuki T. Angle-resolved photoemission spectroscopy of liquid water at 29.5 eV. *Struct. Dyn*. 2017; 4: 044014. https://doi.org/10.1063/1.4979857.

[62] Hartweg S, Yodr BL, Garcia GA, Hahon L, Signorell R. Size-Resolved Photoelectron Anisotropy of Gas Phase Water Clusters and Predictions for Liquid Water. Phys. Rev. Lett. 2017; 118: 103402. https://link.aps.org/doi/10.1103/PhysRevLett.118.103402.

[63] Signorell R, Goldman L, Yoder BL, Bodi A, Chasovskikh. Nanofocusing, shadowing,

and electron mean free path in the photoemission from aerosol droplets. *Chem. Phys. Lett.* 2016; 658;1. https://doi.org/10.1016/j.cplett.2016.05.046.

[64] Michaud M, Wen A, Sanche L. Cross Sections for Low-Energy (1–100 eV) Electron Elastic and Inelastic Scattering in Amorphous Ice. *Radiat. Res*. 2003; 159: 3. https://doi.org/10.1667/0033-7587(2003)159[0003:CSFLEE]2.0.CO;2

[65] Michaud M, Sanche L. Total cross sections for slow-electron (1–20 eV) scattering in solid H_2O. *Phys. Rev. A.*, 1987; 36: 4672. https://doi.org/10.1103/PhysRevA.36.

[66] Olivieri G, Parry KM, D'Auria R, Tobias DJ, Brown MA. Specific anion effects at the aqueous solution-air interface: MD simulations, SESSA calculations, and photoelectron spectroscopy experiments. *J. Phys. Chem. B*. 2018; 122: 910-918. https://doi.org/10.1021/acs.jpcb.7b06981.

[67] Werner WSM., Smekal W, Powell CJ, NIST Database for the Simulation of Electron Spectra for Surface Analysis (SESSA), Version 2.0, Standard Reference Data program SRD 100, U.S. Department of Commerce, National Institute of Standards and technology, Gaithersburg, MD, 2014.

[68] Werner WSM, Smekal W, Powell CJ. Simulation of electron spectra for surface analysis (SESSA): A novel software tool for quantitative Auger-electron spectroscopy of X-ray photoelectron spectroscopy. *Surf. Interface Anal.* 2005; 37: 1059-1067. https://doi.org/10.1002/sia.2097

[69] Emfietzoglou D, Kyriakou I, Garcia-Molina R, Abril I. Inelastic mean free paths of low-energy electrons in condensed media: Beyond the standard models. *Surf. Interface Anal*. 2017: 49; 4-10.

[70] Tung CJ, Chao TC, Hsieh HW, Chan WT. Low-energy electron interactions with liquid water and energy deposition in nanometric volumes. *Nucl. Instr. Methods Phys. Res. B*. 2007; 262: 231-239. https://doi.org/10.1016/j.nimb.2007.05.023

[71] Dupuy ZR, Richter C, Winter B, Meijer G, Schlogl R, Bluhm H. Core level photoelectron spectroscopy of heterogeneous reactions at liquid-vapor interfaces: Current status, challenges, and prospects. *J. Chem. Phys.* 2021; 154: 060901. https://doi.org/10.1063/5.0036178

[72] https://www.dupont.com/content/dam/dupont/amer/us/en/products/ei-transformation/documents/DEC-Kapton-HN-datasheet.pdf

[73] Painter LR, Arakawa ET, Williams MW, Ashley JC. Optical Properties of Polyethylene: Measurement and Applications. Radiat. Res. 1980; 83: 1-18. https://doi.org/10.2307/3575254

[74] Ritsko JJ, Brillson LJ, Bigelow RW, Fabish TJ. Electron energy loss spectroscopy and the optical properties of polymethylmethacrylate from 1 to 300 eV. *The Journal of Chemical Physics.*1978; 69(9): 3931-3939. https://doi.org/10.1063/1.437131

[75] Shimamura, K.; Karasz, Frank E.; Hirsch, Jacob A.; Chien, James C. W. Crystal structure of *trans*-polyacetylene. Makromolekulare Chemie. Rapid Communications. 1981; 2: 473-480. https://doi.org/10.1002/marc.1981.030020801

76 Okabe T, Characteristic Energy Loss Spectra and Optical Constants of Some Solid Hydrocarbons. *J. Phys. Soc. J*apan 1973;35(5): 1496 – 1500. https://doi.org/10.1143/JPSJ.35.1496.

[77] Arakawa ET, Emerson LC, Juan I, Ashley JC, Williams MW. The Optical properties of Adenine form. *Photochemistry and Photobiology*. 1986; 44(3): 349-353. https://doi.org/10.1111/j.1751-1097.1986.tb04674.x

[78] Emerson LC, Williams MW, Tang I, Hamm RN, Arakawa ET. Optical Properties of Guanine from 2 to 82 eV. *Radiation Research*.1975; 63: 235-244. https://doi.org/10.2307/3574149

[79] Arakawa ET, Williams MW, Ashley JC, Painter LR. The optical properties of Kapton: Measurement and applications. *J. Appl. Phys.*1981; 52(5): 3579- 3582. https://doi.org/10.1063/1.329140

[80] Ritsko JJ. Momentum-dependent dielectric function of polyacetylene. *Physical Review* B.1982; 26(4): 2192-2198. https://doi.org/10.1103/PhysRevB.26.2192

[81] Williams MW, Young DW, Ashley JC, Arakawa ET. Optical and electronic properties of the electron beam resist poly(butene-1-sulfone). *J. Appl. Phys*.1985; 58(11): 4360-4364. https://doi.org/10.1063/1.335525

[82] Palik ED. *Handbook of Optical Constants of Solids II*. New York: Academic Press; 1991.

[83] Inagaki T, Arakawa ET, Hamm RN, Williams MW. Optical properties of polystyrene from the near-infrared to the x-ray region and convergence of optical sum rules. *Physical Review B*. 1977; 15(6): 3243-3253. https://doi.org/10.1103/PhysRevB.15.3243

[84] Ritsko JJ, Bigelow. Core excitons and the dielectric response of polystyrene and poly(2-vinylpyridine) from 1 to 400 eV. *J. Chem. Phys*.1978; 69; 4162-4170. https://doi.org/10.1063/1.437096

[85] Isaacson M. I Interaction of 25 keV Electrons with the Interaction of 25 keV Electrons with the Nucleic Acid Bases, Adenine, Thymine, and Uracil. I. Outer shell excitation. *The Journal of Chemical Physics.* 1972; 56: 1803-1812. https://doi.org/10.1063/1.1677456

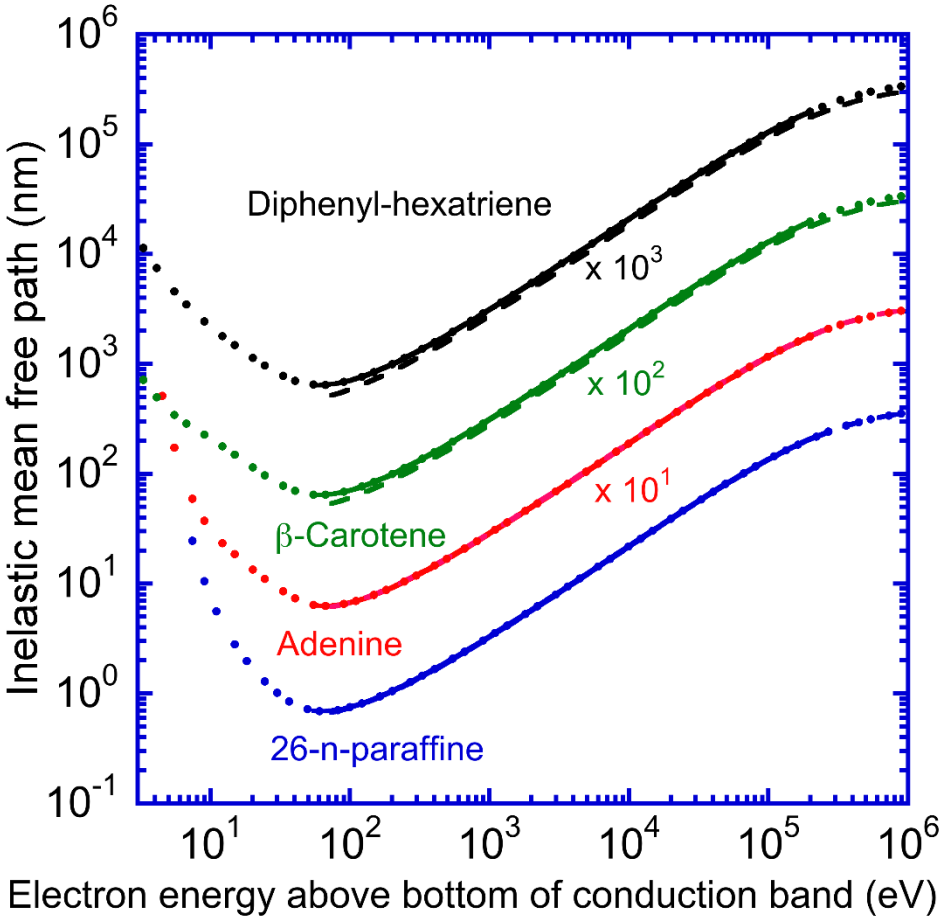

Figure 1.

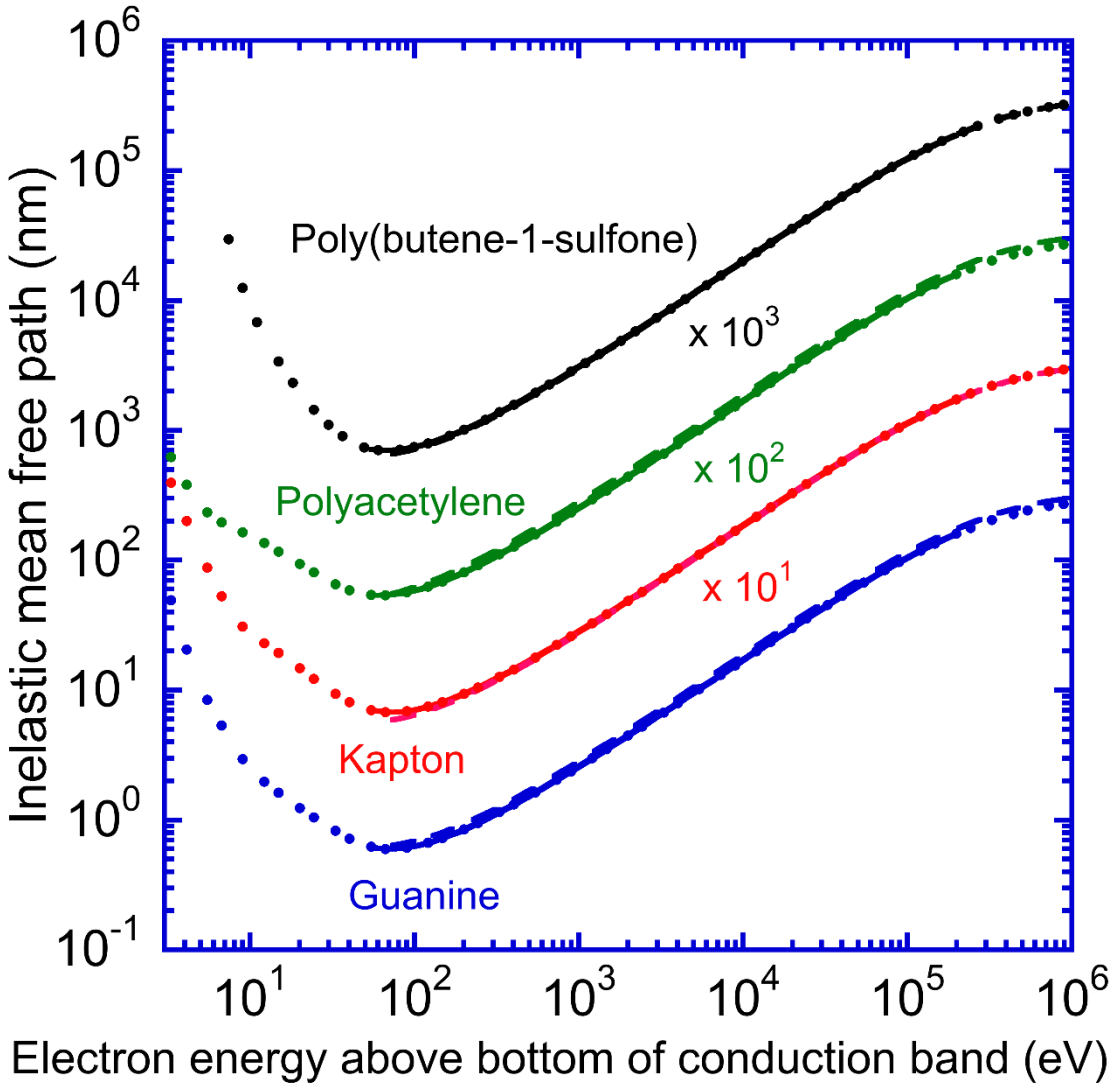

Figure 2.

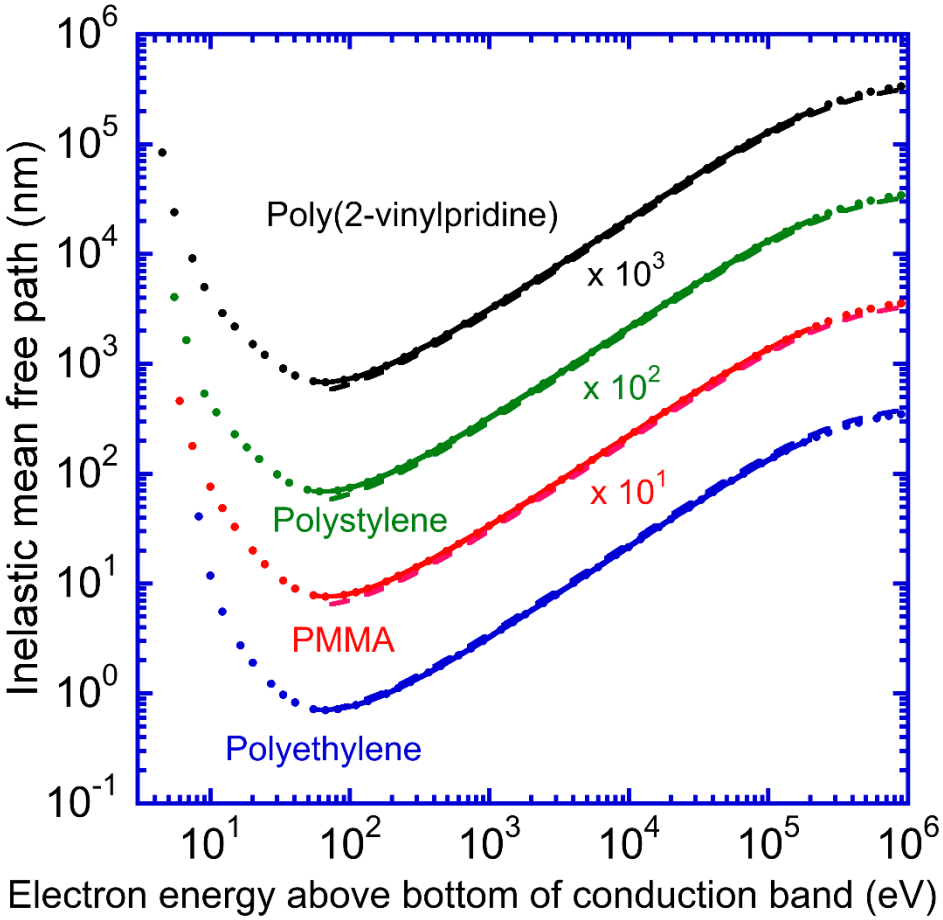

Figure 3.

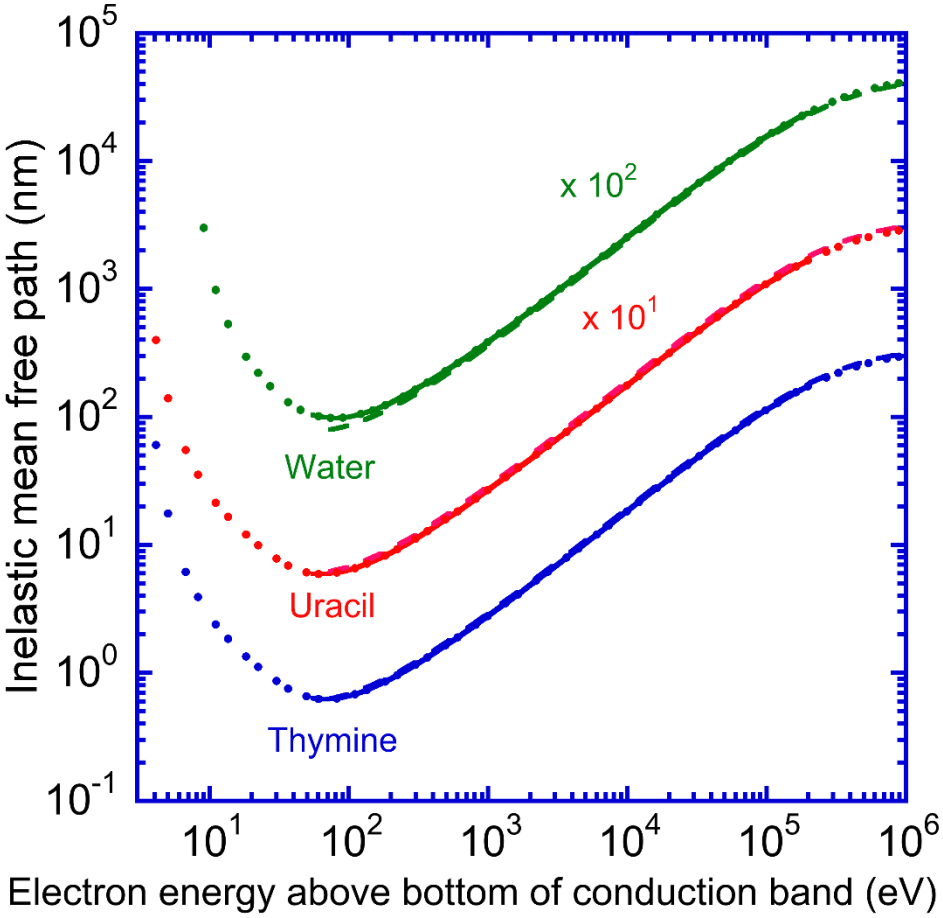

Figure 4.

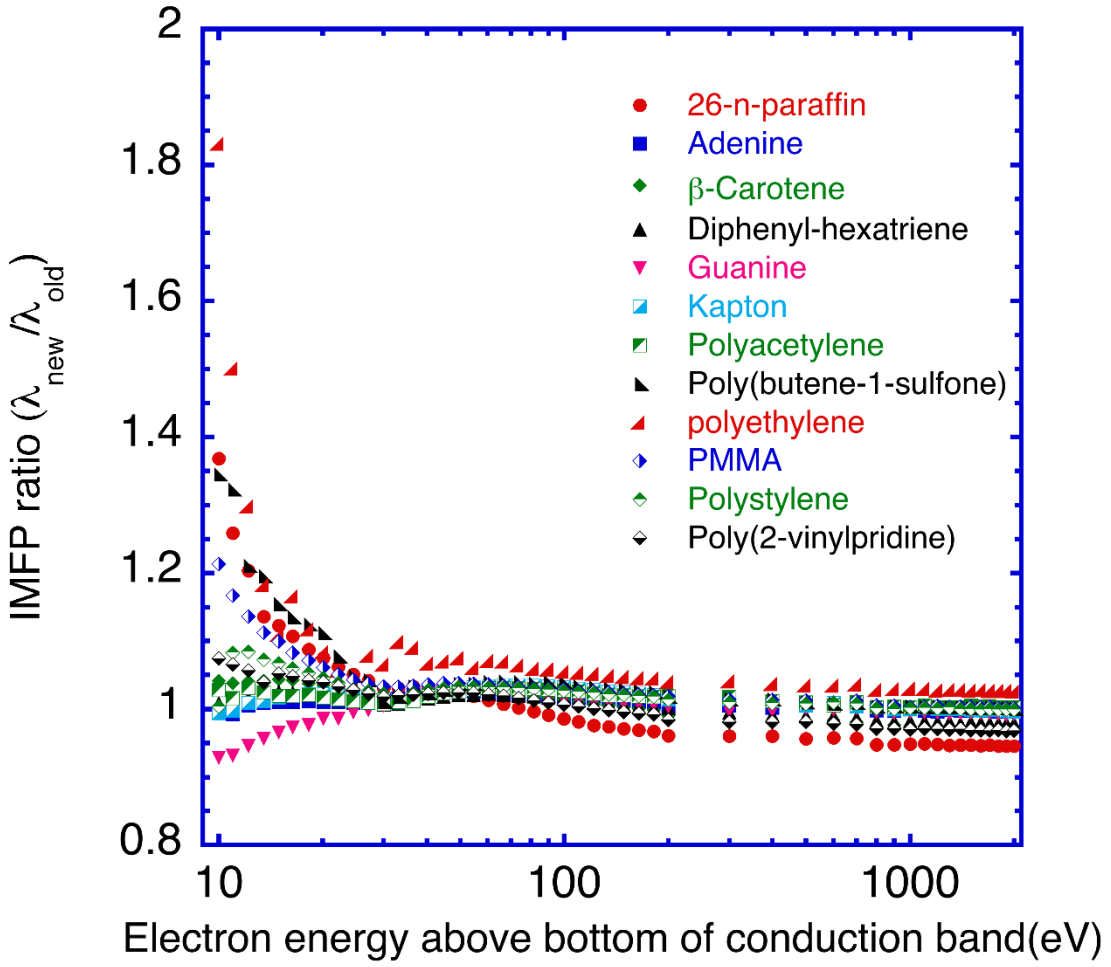

Figure 5

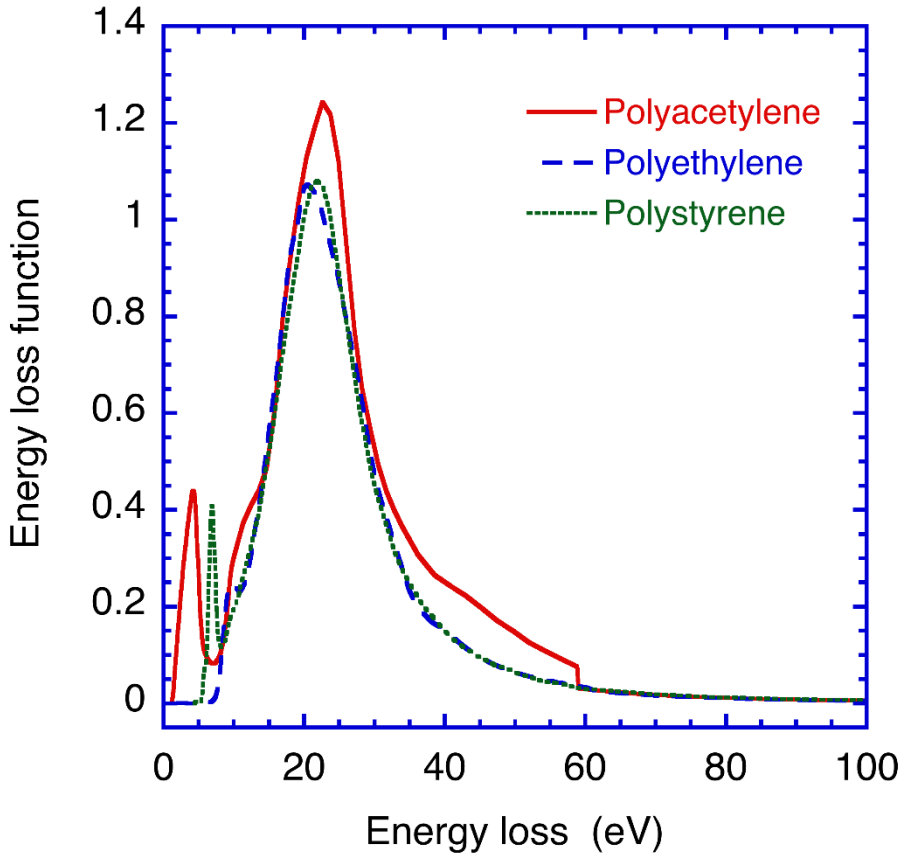

Figure 6

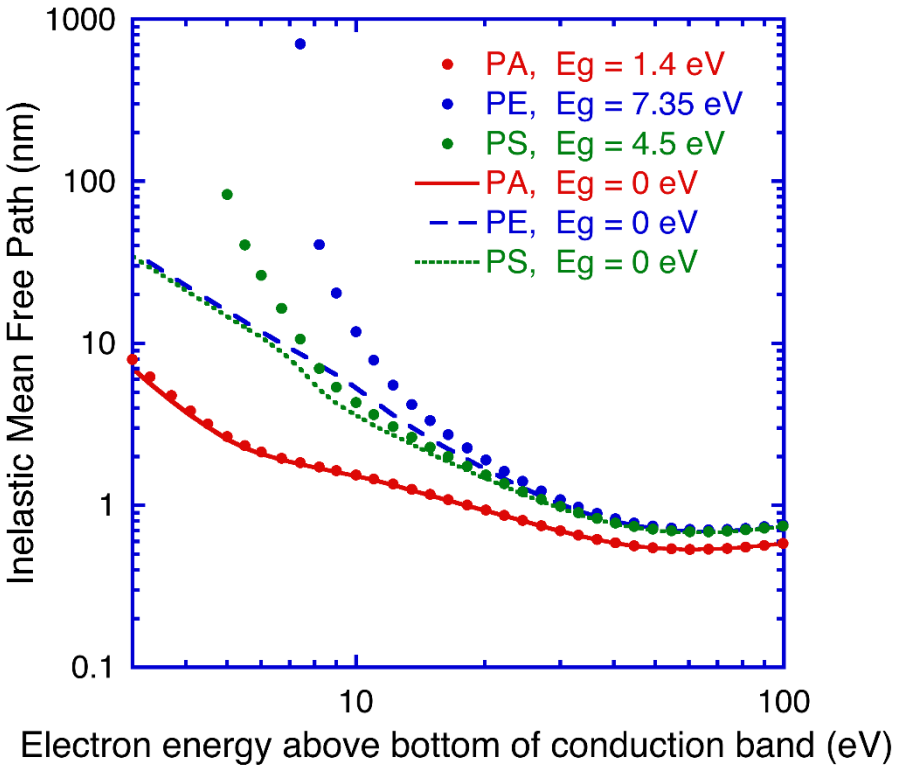

Figure 7

Figure 8

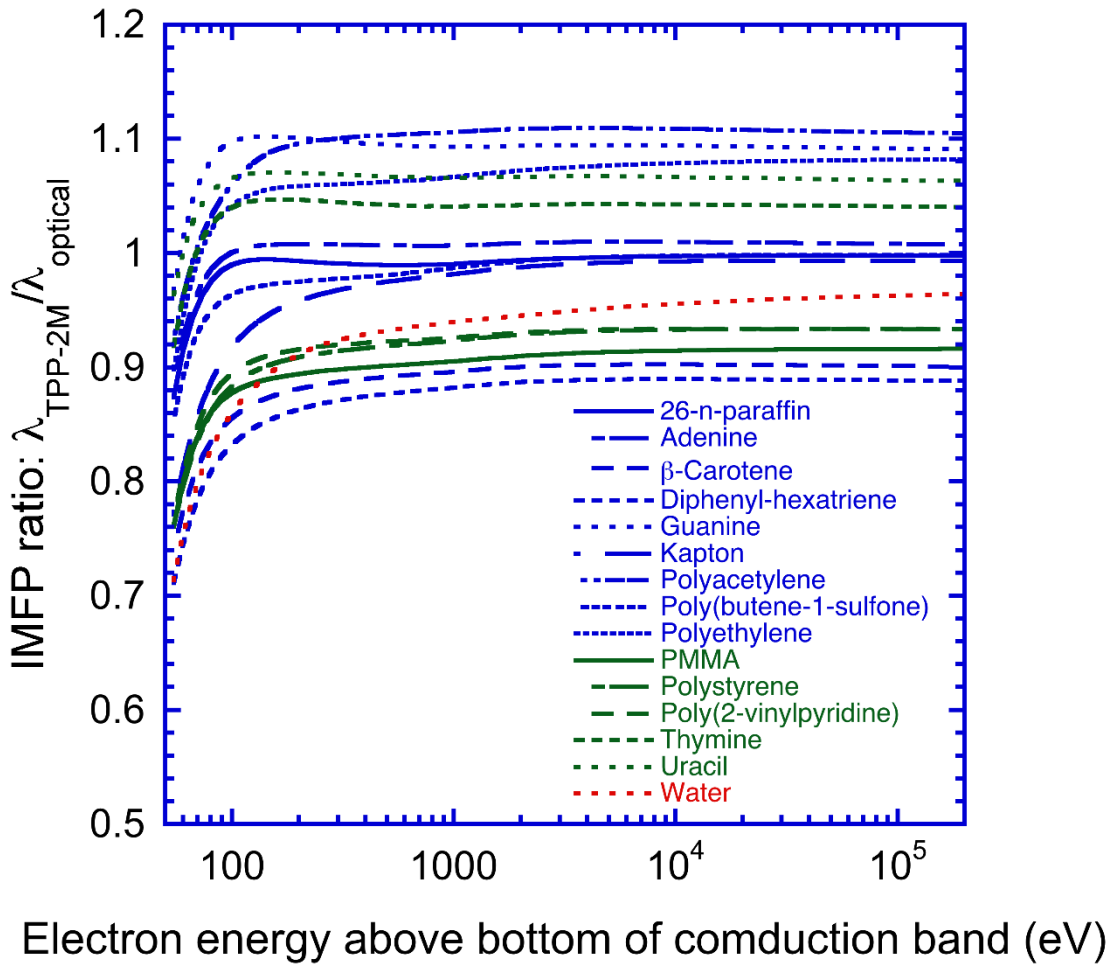

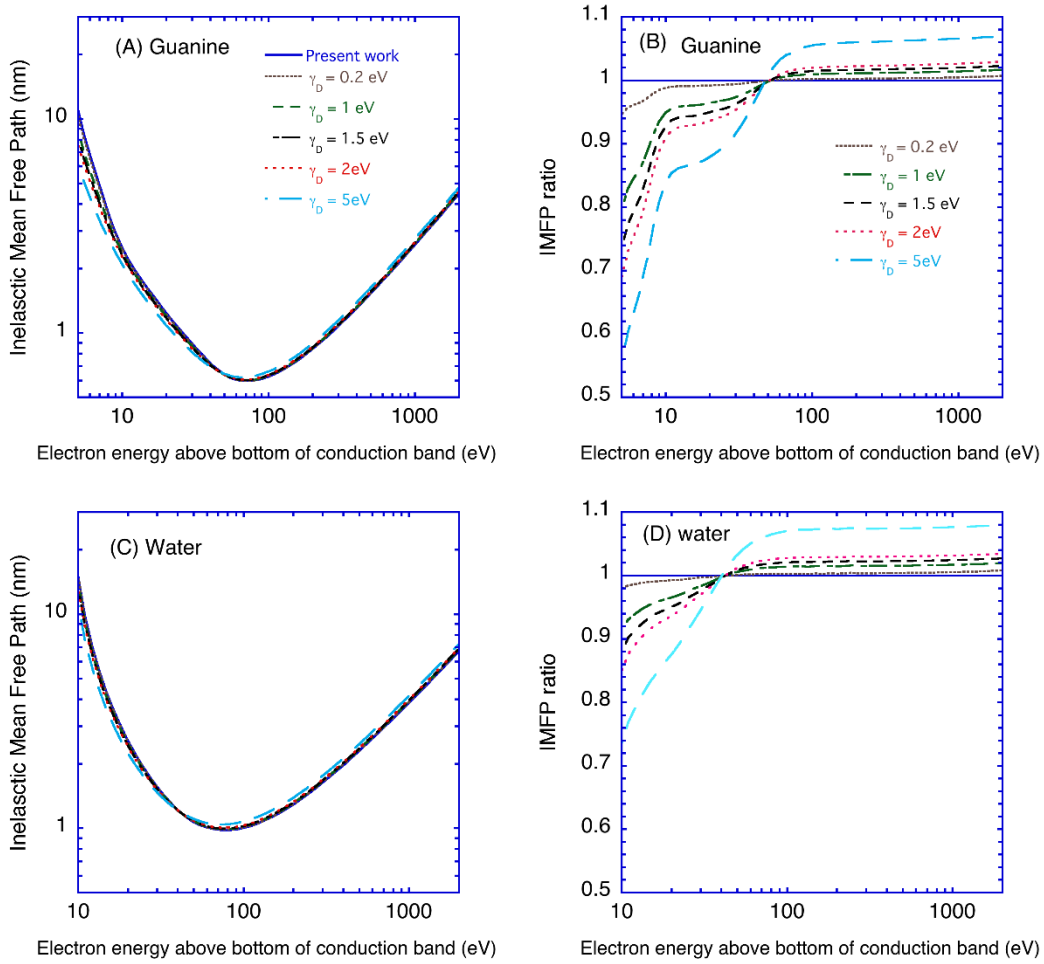

Fig. 9

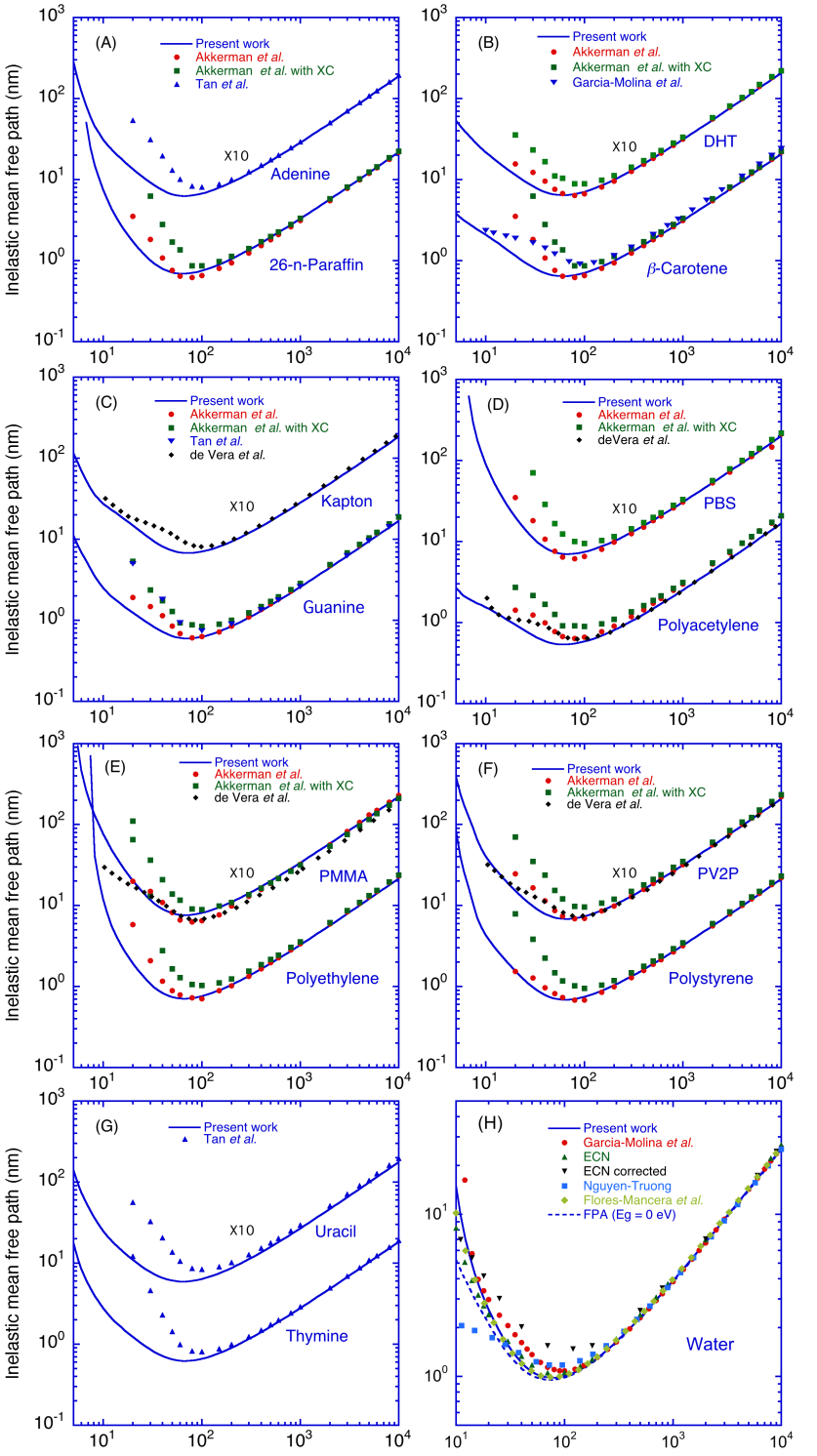

Fig.10

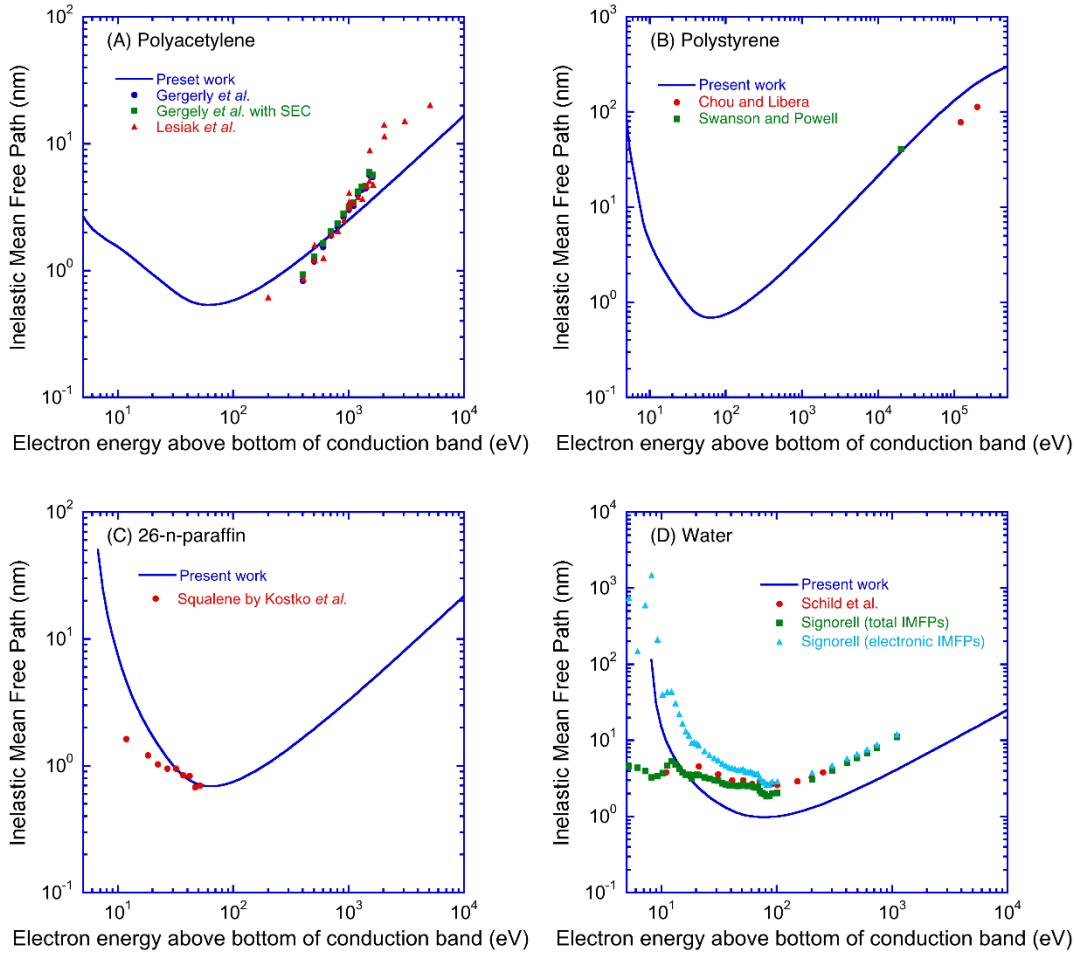

Fig. 11